

# C-metric in a (nut)shell

Cameron R D Bunney<sup>1</sup> and Robert B Mann<sup>2,3</sup>

<sup>1</sup>School of Physics and Astronomy, University of Nottingham, Nottingham NG7 2RD, UK

<sup>2</sup>Department of Physics and Astronomy, University of Waterloo, Waterloo, Ontario, N2L 3G1, Canada

<sup>3</sup>Perimeter Institute for Theoretical Physics, 31 Caroline St., Waterloo, Ontario, N2L 2Y5, Canada

E-mail: [cameron.bunney@nottingham.ac.uk](mailto:cameron.bunney@nottingham.ac.uk), [rbmann@uwaterloo.ca](mailto:rbmann@uwaterloo.ca)

October 2024

**Abstract.** We present a comprehensive study of the C-metric in  $2 + 1$  dimensions, placing it within a shell of stress energy and matching it to an exterior vacuum AdS metric. The  $2 + 1$  C-metric is not circularly symmetric and hence neither are the constructed shells, which instead take on a cuspidal or teardrop shape. We interpret the stress energy of the shells as a perfect fluid, calculating the energy density and pressure. For accelerating particles (Class I), we find the stress energy is concentrated on the part of shell farthest from the direction of acceleration and always respects the strong energy condition. For accelerating black holes (Class I<sub>C</sub>, II, and III), the shell stress energy may either respect or violate the energy conditions depending on the parameter of the exterior metric — between the two regimes lies a critical value of the external parameter for which the shell stress energy vanishes, leading to new solutions of Einstein's field equations, which fall into three categories: an accelerated black hole pulled by a finite-length string with a point particle at the other end, an accelerated black hole pushed by a finite-length strut with a point particle at the other end, and an accelerated black hole pushed from one side by a finite-length strut and pulled from the other by a finite-length string, each with a point particle at the other end.

## 1. Introduction

Accelerating black holes are garnering increased interest in the physics community, in large part because historically the effects of acceleration on the properties of the black hole have not been understood. In four spacetime dimensions these objects are described by the C-metric [1, 2], which is interpreted as the metric of a black hole undergoing uniform acceleration that is isolated from a second black hole by a non-compact acceleration horizon [3, 4]. The acceleration is due to the force from a string of positive tension stretching from infinity to the horizon along the axis of symmetry, pulling the black hole; alternatively it can be due to a strut (of negative tension) pushing the black hole and connecting its horizon to the second black hole. These solutions have been generalised to include a cosmological constant  $\Lambda$  [5, 6, 7], rotation and electromagnetic charge [8], and dilatons [9].

The anti-de Sitter (AdS) case, with  $\Lambda < 0$ , has been of considerable recent attention. In this case, if the acceleration is sufficiently small, the black hole is suspended at a fixed distance from the centre of AdS, and there is neither an acceleration horizon nor a second black hole. In such situations the laws of thermodynamics can be consistently formulated [10, 11, 12], and

applied to uncover new and interesting thermodynamic behaviour [13, 14, 15]. Extensions of the first law to black holes that possess an acceleration horizon have been carried out [16, 17].

Accelerating black holes have proven to be very useful in understanding the quantum properties of black holes [18, 19]. By placing a brane in AdS that slices an accelerating black hole, excising the part of the spacetime containing the string, and then gluing it to a copy of itself, a static black hole solution in (2+1) dimensions (i.e. on the brane) is obtained that takes into account quantum backreaction [20, 21, 22]. This construction is a realisation of the braneworld holography principle: gravity emerges from the brane.

For these reasons, amongst others, it is of interest to consider accelerating black holes in (2+1) dimensions. First discovered in [23], an investigation of such solutions was recently carried out [24, 25] and a rich panoply of solutions obtained. Three classes of (2+1)-dimensional versions of the C-metric were obtained, with different interpretations for each. Uniting each solution was the presence of a domain wall: a thread of stress energy that pulled or pushed the black hole, thereby accelerating it. These solutions straightforwardly generalise to include accelerating point masses [24, 25]. As the wall is one-dimensional, we shall henceforth refer to it as a string (or strut), recognising that in two spatial dimensions this object is actually a domain wall.

Including rotation in such solutions is not straightforward, since a portion of the domain wall beyond a sufficiently large distance from the horizon would have a superluminal rotation velocity. One way of addressing this problem would be to place a rotating black hole inside a shell whose size is small enough to ensure such superluminal motion does not occur.

Motivated by this we consider here the problem of placing a non-rotating black hole inside a shell of stress-energy. We find a range of solutions that is as rich – or even richer – as those for the C-metric. Shells in general take the form of cardioids or teardrops, depending on the parameters of the interior metric. The metric outside the shell is that of a static AdS spacetime for either a black hole or a point mass; which of these is realised likewise depends on the parameters of the solution.

Our approach is in some sense complementary to the problem of Oppenheimer-Snyder collapse [26] in (2+1) dimensions [27]. Rather than assume circular symmetry and a dynamically collapsing shell [28], we assume a static shell but not circular symmetry.

The outline of our paper is as follows. We begin in Section 2 by developing the general formalism for placing the C-metric inside a shell, computing the junction conditions and the resultant density and pressure of the shell. Both of these quantities depend on the angular location of a Section of the shell relative to the domain wall axis: essentially the stress energy collects away from the direction of acceleration. In Section 3, we construct shells for the first class of black holes pulled by a string and in Section 4 for those pulled by a strut. The two situations are similar, but not symmetric. In the next two sections, we carry out the shell construction for the second class of accelerating black holes that are either pushed (Section 5) or pulled (Section 6). In Section 7, we consider shell construction for the third class, which hitherto has received relatively little attention. We summarise our work in a concluding section.

## 2. C-metric in a shell

There are three classes of C-metric, each with its own interpretation. Class I represents an accelerated particle and Class II an accelerated BTZ black hole, pushed or pulled by a strut. Class III does not have an interpretation in terms of particle-like or black-hole-like solutions.

Class	$Q(x)$	$P(y)$	Maximal range of $x$
I	$1 - x^2$	$\frac{1}{A^2\ell^2} + (y^2 - 1)$	$ x  < 1$
II	$x^2 - 1$	$\frac{1}{A^2\ell^2} + (1 - y^2)$	$x > 1$ or $x < -1$
III	$1 + x^2$	$\frac{1}{A^2\ell^2} - (1 + y^2)$	$\mathbb{R}$

Table 1: The three classes of C-metric solutions in prolate coordinates  $(x, y)$ , each with its maximal range of  $x$ .  $\ell$  is the AdS length scale.

We confine the C-metric within a shell with an asymptotically-AdS spacetime outside the shell absent of any topological defects.

### 2.1. C-metric

We present first the C-metric in prolate coordinates [24, 25, 29],

$$ds^2 = \frac{1}{\Omega^2(x, y)} \left( -P(y)d\tau^2 + \frac{dy^2}{P(y)} + \frac{dx^2}{Q(x)} \right), \quad (2.1)$$

$$\Omega(x, y) = A(x - y), \quad (2.2)$$

where  $A$  is an acceleration parameter and  $P$  and  $Q$  are polynomials. There are three distinct classes of C-metric, summarised in Table 1. Class I represents accelerating particle-like solutions, and has a subclass dubbed  $I_C$ , representing an accelerated black-hole solution [24]. Class II represents an accelerated black hole and is a one-parameter extension of the BTZ geometry but is disconnected from the Class  $I_C$  black-hole solution. Class III has neither a particle-like nor a black-hole-like interpretation.

It is more intuitive to work in polar coordinates  $(\sigma, r, \phi)$ ,

$$\tau = \frac{m^2 \mathcal{A} \sigma}{\alpha}, \quad (2.3a)$$

$$y = -\frac{1}{\mathcal{A} r}, \quad (2.3b)$$

$$x = \begin{cases} \cos(m\phi) & \text{Class I } (0 \leq m < 1), \\ \cosh(m\phi) & \text{Class II } (m > 0), \\ \sinh(m\phi) & \text{Class III } (m \in \mathbb{R}), \end{cases} \quad (2.3c)$$

where  $\mathcal{A} = A/m$  and  $\alpha$  and  $m$  are dimensionless parameters. To ensure that the C-metric [24] solves the Einstein equations everywhere, a domain wall is inserted at  $\phi = \pm\pi$ . This ensures the necessary force for acceleration. We refer to the domain wall as a string if it has positive tension and a strut if it has negative tension. In these coordinates, the C-metric reads

$$ds^2 = \frac{1}{\Omega^2(r, \phi)} \left( -\frac{f(r)}{\alpha^2} d\sigma^2 + \frac{dr^2}{f(r)} + r^2 d\phi^2 \right), \quad (2.4)$$

where  $f(r)$  and  $\Omega(r, \phi)$  are given in Table 2 for the three classes of C-metric. Conformal infinity is found at the zeros of  $\Omega$ .

## 2.2. BTZ black holes and point particles

In the next section, we will construct a shell of stress energy around the C-metric described in Section 2.1. In this section, we describe the geometry exterior to the shell, which we require to be the spacetime of constant negative curvature with mass parameter  $M$  [30, 31, 32]. In Schwarzschild-like coordinates, this metric reads

$$ds_+^2 = -g(r_+)dt^2 + \frac{dr_+^2}{g(r_+)} + r_+^2 d\theta^2, \quad (2.5a)$$

$$g(r_+) = \frac{r_+^2}{\ell^2} - M, \quad (2.5b)$$

where  $M$  is a dimensionless mass parameter and  $\ell$  is the AdS length scale. When  $\theta$  is  $2\pi$  periodic,  $M$  is the ADM mass of the spacetime [30].

There are four distinct physical interpretations of the metric (2.5), depending on the value of  $M$  [33]: for  $M \geq 0$ , the metric (2.5) describes a spinless black hole; for  $-1 < M < 0$ , the metric (2.5) has an angular defect, interpreted as a particle of positive mass at the centre of the spacetime; for  $M = -1$ , the metric (2.5) describes global anti-de Sitter spacetime; and for  $M < -1$ , the metric (2.5) has an angular excess, interpreted as a particle of negative mass at the centre of the spacetime.

We comment briefly now on the transition between the black-hole-like and particle-like solutions at  $M = 0$ . For  $M = 0$ , the metric (2.5) reads

$$ds_+^2 = -\frac{r_+^2}{\ell^2} dt^2 + \ell^2 \frac{dr_+^2}{r_+^2} + r_+^2 d\theta^2. \quad (2.6)$$

Introducing  $t' = t/\ell$ ,  $z = \ell/r_+$ , the metric (2.6) reduces

$$ds_+^2 = \frac{\ell^2}{z^2} \left( -dt'^2 + dz^2 + d\theta^2 \right), \quad (2.7)$$

where  $z > 0$ .

As  $\theta$  is identified, the geometry of (2.7) is that of Torricelli's trumpet or Gabriel's horn and is conformally a half-cylinder (as  $z > 0$ ). If  $\theta$ , however, were not identified ( $-\infty < \theta < \infty$ ), the geometry would instead be that of the Poincaré patch of AdS.

## 2.3. Shell construction

We now consider a spacetime separated into two regions  $\mathcal{V}^+$  and  $\mathcal{V}^-$  by a hypersurface  $\Sigma$ . Throughout this section, we denote spacetime indices using Greek indices and hypersurface indices with Latin indices. In the region  $\mathcal{V}^-$  interior to the shell, we consider in turn each class of the C-metric (2.4). In the exterior region  $\mathcal{V}^+$ , we take the geometry described in Section 2.2.

Class	$f(r)$	$\Omega(r, \phi)$
I	$\frac{r^2}{\ell^2} + m^2(1 - \mathcal{A}^2 r^2)$	$1 + \mathcal{A}r \cos(m\phi)$
II	$\frac{r^2}{\ell^2} - m^2(1 - \mathcal{A}^2 r^2)$	$1 + \mathcal{A}r \cosh(m\phi)$
III	$\frac{r^2}{\ell^2} - m^2(1 + \mathcal{A}^2 r^2)$	$1 + \mathcal{A}r \sinh(m\phi)$

Table 2: Three classes of C-metric solutions in polar coordinates.

Coordinates within  $\mathcal{V}^-$  are the  $(\sigma, r, \phi)$ , coordinates of (2.4), within  $\mathcal{V}^+$  are the  $(t, r_+, \theta)$  coordinates of (2.5), and on  $\Sigma$  are  $(\sigma, \phi)$ .

The hypersurface  $\Sigma$  is placed at  $(\sigma, r, \phi) = (\sigma, r_0, \phi)$  in the region  $\mathcal{V}^-$ , and in the region  $\mathcal{V}^+$  at  $(t, r_+, \theta) = (\sigma, R_M(\phi), \Theta_M(\phi))$ , where  $\phi$  is the inner angular coordinate  $\phi \in (-\pi, \pi)$  and the subscript  $M$  makes the  $M$ -dependence explicit. The induced metric on  $\Sigma$  is then

$$ds_+^2|_{\Sigma} = g_{\mu\nu}^+ dx^\mu dx^\nu|_{\Sigma} = - \left( \frac{R_M^2}{\ell^2} - M \right) d\sigma^2 + \left( \frac{\ell^2 \dot{R}_M^2}{R_M^2 - M\ell^2} + R_M^2 \dot{\Theta}_M^2 \right) d\phi^2, \quad (2.8a)$$

$$ds_-^2|_{\Sigma} = g_{\mu\nu}^- dx^\mu dx^\nu|_{\Sigma} = \frac{1}{\Omega^2(r_0, \phi)} \left( -\frac{f(r_0)}{\alpha^2} d\sigma^2 + r_0^2 d\phi^2 \right), \quad (2.8b)$$

in the respective  $\mathcal{V}^+$  and  $\mathcal{V}^-$  coordinates, where  $f(r)$  and  $\Omega(r, \phi)$  are given in Table 2 for the three classes of C-metric and an overdot denotes a derivative with respect to  $\phi$ .

The metrics in (2.8) must match, as required by the first junction condition [34]. By comparing the coefficients of  $d\sigma^2$  and  $d\phi^2$ , this yields expressions for  $R_M$  and  $\Theta_M$

$$R_M(\phi) = \ell \sqrt{\frac{f(r_0)}{\alpha^2} \frac{1}{\Omega^2(r_0, \phi)} + M}, \quad (2.9a)$$

$$\Theta_M(\phi) = \int_0^\phi d\phi' \frac{1}{R_M(\phi')} \sqrt{\frac{r_0^2}{\Omega^2(r_0, \phi')} - \frac{\ell^2 \dot{R}_M^2(\phi')}{R_M^2(\phi') - M\ell^2}}. \quad (2.9b)$$

in terms of the interior coordinate  $\phi$ .

For a well-defined shell, the arguments of the square roots in (2.9) must be positive. A necessary and sufficient condition for this is the non negativity of the argument in the square root of (2.9b), which imposes a constraint on the possible values of  $M$

$$M \geq M_{\min} = \frac{f(r_0)}{\alpha^2} \frac{1}{\Omega^2(r_0, \phi_*)} \left( \frac{\ell^2}{r_0^2} \dot{\Omega}^2(r_0, \phi_*) - 1 \right), \quad (2.10)$$

for a given pair  $(r_0, \alpha)$ , where  $\phi_* \in [-\pi, \pi]$  is the value of  $\phi$  maximising the right-hand side of (2.10).

Using the second junction condition, we interpret the hypersurface as a thin shell of stress energy, governed by the Lanczos equation [34],

$$S_{ab} = -\frac{1}{8\pi} ([K_{ab}] - [K] h_{ab}), \quad (2.11)$$

where  $K_{ab}$  is the extrinsic curvature,  $h_{ab}$  is the induced metric on  $\Sigma$ ,  $K = h^{ab} K_{ab}$ , and the square bracket notation means  $[A] = A(\mathcal{V}^+)|_{\Sigma} - A(\mathcal{V}^-)|_{\Sigma} = A^+|_{\Sigma} - A^-|_{\Sigma}$  for any tensorial quantity  $A$ .

Projecting from  $\mathcal{V}^\pm$  to  $\Sigma$  yields the induced metric

$$h_{ab} = g_{\mu\nu}^\pm|_{\Sigma} e^{\pm\mu}_a e^{\pm\nu}_b, \quad (2.12)$$

where

$$e_\sigma^- = (1, 0, 0), \quad e_\phi^- = (0, 0, 1), \quad (2.13a)$$

$$e_\sigma^+ = (1, 0, 0), \quad e_\phi^+ = (0, \dot{R}_M, \dot{\Theta}_M) =: v^{+\mu}, \quad (2.13b)$$

and  $v^{+\mu}$  is the tangent vector to  $\Sigma$  in  $\mathcal{V}^+$ . The extrinsic curvature is then given by

$$K_{ab}^\pm = (\nabla_\mu n_\nu^\pm)|_{\Sigma} e^{\pm\mu}_a e^{\pm\nu}_b, \quad (2.14)$$

where  $n_\mu^\pm$  is the normal to  $\Sigma$  in  $\mathcal{V}^\pm$  such that  $n^{\pm\mu}n^\pm_\mu = 1$ ,

$$n_\mu^- = k^-(\phi)(0, 1, 0), \quad k^-(\phi) = \frac{1}{\sqrt{f(r_0)\Omega(r_0, \phi)}}, \quad (2.15a)$$

$$n_\mu^+ = k^+(\phi)(0, \dot{\Theta}_M, -\dot{R}_M), \quad k^+(\phi) = \frac{1}{\sqrt{g(R_M)\dot{\Theta}_M^2 + \dot{R}_M^2/R_M^2}} \quad (2.15b)$$

and  $v^{+\mu}n_\mu^+ = 0$ . We note in passing that in the thin-shell approach to Oppenheimer-Snyder collapse [26], one relaxes the assumption of staticity of the shell but assumes circular symmetry. In the present formulation, we assume staticity without circular symmetry. As such, the calculations in this formulation have strong parallels with those in the collapse of a uniform thin shell.

The nonzero components of the extrinsic curvature are

$$K_{\sigma\sigma}^- = -k^-(\phi)\Gamma_{\sigma\sigma}^r|_\Sigma, \quad K_{\phi\phi}^- = -k^-(\phi)\Gamma_{\phi\phi}^r|_\Sigma, \quad (2.16a)$$

$$K_{\sigma\sigma}^+ = -k^+(\phi)\dot{\Theta}_M\Gamma_{tt}^{r+}|_\Sigma, \quad K_{\phi\phi}^+ = -n_\mu^+\frac{Dv^{+\mu}}{D\phi}\Big|_\Sigma, \quad (2.16b)$$

where

$$\Gamma_{\phi\phi}^r|_\Sigma = -\frac{r_0 f(r_0)}{\Omega(r_0, \phi)}, \quad \Gamma_{\sigma\sigma}^r|_\Sigma = \frac{f(r_0)}{2\alpha^2\Omega(r_0, \phi)}(f'(r_0)\Omega(r_0, \phi) - 2f(r_0)\Omega'(r_0, \phi)), \quad (2.17a)$$

$$\Gamma_{r+r+}^{r+}|_\Sigma = -\frac{R_M}{\ell^2}\frac{1}{g(R_M)}, \quad \Gamma_{\theta\theta}^{r+}|_\Sigma = -R_M g(R_M), \quad \Gamma_{\theta r+}^\theta|_\Sigma = \frac{1}{R_M}, \quad \Gamma_{tt}^{r+}|_\Sigma = \frac{R_M}{\ell^2}g(R_M), \quad (2.17b)$$

are the relevant nonzero Christoffel symbols on  $\mathcal{V}^\pm$ , with  $g$  given in (2.5) and  $f'(r_0) = \partial_r f(r)|_{r=r_0}$  and  $\Omega'(r_0, \phi) = \partial_r \Omega(r, \phi)|_{r=r_0}$ ; both of these latter quantities can be obtained from Table 2. Noting for any vector  $A^\mu$  that  $\frac{DA^\mu}{D\phi} = \frac{dA^\mu}{d\phi} + v^{+\alpha}\Gamma_{\alpha\beta}^\mu A^\beta$ , we obtain

$$K_{\phi\phi}^+ = -k^+(\phi)\left(\dot{\Theta}_M\ddot{R}_M - \ddot{\Theta}_M\dot{R}_M + \dot{\Theta}_M\dot{R}_M^2\Gamma_{r+r+}^{r+}|_\Sigma + \dot{\Theta}_M^3\Gamma_{\theta\theta}^{r+}|_\Sigma - 2\dot{\Theta}_M\dot{R}_M^2\Gamma_{\theta r+}^\theta|_\Sigma\right). \quad (2.18)$$

Using the following relations

$$K_{\sigma\sigma}^\pm - K^\pm h_{\sigma\sigma} = -h_{\sigma\sigma}h^{\phi\phi}K_{\phi\phi}^\pm, \quad K_{\phi\phi}^\pm - K^\pm h_{\phi\phi} = -h_{\phi\phi}h^{\sigma\sigma}K_{\sigma\sigma}^\pm, \quad (2.19)$$

which follow from the definition  $K^\pm = h^{ab}K_{ab}$ , we find the nonzero components of the Lanczos equations (2.11),

$$S_{\sigma\sigma} = \frac{h_{\sigma\sigma}h^{\phi\phi}}{8\pi}(K_{\phi\phi}^+ - K_{\phi\phi}^-), \quad (2.20a)$$

$$S_{\phi\phi} = \frac{h_{\phi\phi}h^{\sigma\sigma}}{8\pi}(K_{\sigma\sigma}^+ - K_{\sigma\sigma}^-), \quad (2.20b)$$

We interpret the stress energy of the shell as a perfect fluid,

$$S^{ab} = (\rho + p)u^a u^b + p h^{ab}, \quad (2.21)$$

where  $u^a$  is the two-velocity of an observer on  $\Sigma$ ,  $\rho$  is the energy density of the shell, and  $p$  is the pressure of the shell. Since the shell is static, we have

$$u^a = \frac{\alpha\Omega(r_0, \phi)}{\sqrt{f(r_0)}}(1, 0), \quad (2.22)$$

implying

$$\rho(\phi) = -h^{\sigma\sigma}S_{\sigma\sigma}, \quad p(\phi) = h^{\phi\phi}S_{\phi\phi}, \quad (2.23)$$

for the respective density and pressure of the shell.

#### 2.4. String ends and point particles

Both the interior and exterior spacetimes are formed by an identification of the angular coordinate, introducing a string in the interior spacetime. We consider now the point at which the string meets the shell. In the Class I and II solutions, there is a single string at the point of identification  $\phi = \pm\pi$ . We may calculate the presence of an angular deficit or excess by considering the angle made between a tangent to the shell and a line of constant angle, along which the identifications are made.

In the interior spacetime, the tangent vector to  $\phi = \text{constant}$  is given by  $v^{-\mu} \propto (0, 1, 0)$ , whereas the tangent to the shell at  $r = r_0$  is given by  $u^{-\mu} \propto (0, 0, 1)$ . These vectors are clearly orthogonal, and so the angle between the shell and the line  $\phi = \pi$  is  $\pi/2$  and the angle between the shell and the line  $\phi = -\pi$  is  $\pi/2$ .

We consider now the same calculation for the exterior spacetime. The corresponding tangent vectors are given by

$$v^{+\mu} = \kappa_1(0, 1, 0), \quad u^{+\mu} = \kappa_2(0, \mp \dot{R}_M(\pm\pi), \dot{\Theta}_M(\pm\pi)), \quad (2.24)$$

at  $\phi = \pm\pi$ . The normalisation functions  $\kappa_1$  and  $\kappa_2$  are given by

$$\kappa_1 = \sqrt{g(R_M(\pm\pi))}, \quad \kappa_2 = \frac{1}{\sqrt{h_{\phi\phi}(\pm\pi)}}, \quad (2.25)$$

where  $g(R)$  and  $h_{\phi\phi}(\phi)$  are given by (2.8). We note that  $\dot{R}_M$  is an odd function of its argument, whereas  $\dot{\Theta}_M$ ,  $R_M$  and  $h_{\phi\phi}$  are even functions. As such, we see that the tangent vectors (2.24) at  $\phi = \pm\pi$  are the same. In particular, the angle between the two tangents at  $\phi = \pi$  and  $\phi = -\pi$  is the same. The angle between the tangents at  $\phi = \pm\pi$  and the tangent to the shell is given by

$$\cos(\Delta) = -\frac{\dot{R}_M(\pi)}{\sqrt{h_{\phi\phi}(\pi)g(R_M(\pi))}} = -\frac{\dot{R}_M(\pi)}{\sqrt{-h_{\phi\phi}(\pi)h_{\sigma\sigma}(\pi)}}, \quad (2.26)$$

where  $h_{\sigma\sigma}$  is given by (2.8).

The total angle  $\delta$  around the point  $\phi = \pm\pi$  on the shell is given by  $\delta = \pi + 2\Delta$ , which may be rewritten as

$$\delta = 2\pi\gamma, \quad (2.27a)$$

$$\gamma = \frac{1}{2} + \frac{1}{\pi} \arccos\left(-\frac{\dot{R}_M(\pi)}{\sqrt{-h_{\phi\phi}(\pi)h_{\sigma\sigma}(\pi)}}\right). \quad (2.27b)$$

This angular deficit ( $\gamma < 1$ ) or excess ( $\gamma > 1$ ) arises from the absence of circular symmetry in the shell. For a circularly symmetric shell, we have  $R_M = \text{const}$ ,  $\dot{R}_M = 0$ , in which case we have  $\gamma = 1$ ,  $\delta = 2\pi$ . This angular deficit or excess may be interpreted as a point mass [35] lying at the end of the string, with mass

$$\mu_\pi = \frac{1}{4}(1 - \gamma). \quad (2.28)$$

For angular deficits, this point particle has positive mass, whereas for angular excesses, the point particle has negative mass. We recall that for  $z \in (-1, 0)$ ,  $\arccos z \in (\frac{\pi}{2}, \pi)$  and for  $z \in (0, 1)$ ,  $\arccos z \in (0, \frac{\pi}{2})$ . Furthermore, in Class I and II,  $\dot{R}_M$  is proportional to  $\mathcal{A}$ . As Class I<sub>pulled</sub>/II<sub>left</sub> is related to Class I<sub>pushed</sub>/II<sub>right</sub> by mapping  $\mathcal{A} \rightarrow -\mathcal{A}$ , we therefore see that an

angular deficit/excess in one corresponds to an angular excess/deficit in the other. Note that this is consistent with the change in sign of the string tension as  $\mathcal{A} \rightarrow -\mathcal{A}$  [24, 25].

In Section 7, we construct a double-string solution, which contains an additional string at  $\phi = 0$ . This spacetime is constructed by taking two copies of the Class III spacetime in the interval  $\phi \in (0, \pi)$ , relabelling the angular coordinate in the second by  $\phi \rightarrow -\phi$  and gluing the two copies at  $\phi = 0$  and  $\phi = \pm\pi$ . In this construction, we use two copies of the spacetime and simply relabel the angular coordinate in one copy. As such, the angle between  $\phi = 0$  and the shell is the same in both copies of the spacetime, as is the angle between  $\phi = \pm\pi$  and the shell. The tangent vectors at  $\phi = \pi$  are given by (2.24) and the tangent vectors at  $\phi = 0$  are given by

$$V^{+\mu} = k_1(0, 1, 0), \quad U^{+\mu} = k_2(0, \dot{R}_M(0), \dot{\Theta}_M(0)), \quad (2.29)$$

where

$$k_1 = \sqrt{g(R_M(0))}, \quad k_2 = \frac{1}{\sqrt{h_{\phi\phi}(0)}}. \quad (2.30)$$

As in the Class I and II calculations above, the angle at  $\phi = 0$  and  $\phi = \pm\pi$  in the interior metric is given by  $\pi/2$ . Hence, the angle between the tangent at  $\phi = \pm\pi$  and the tangent to the shell is again given by (2.26) and (2.27), whereas the angle between the tangent at  $\phi = 0$  and the tangent to the shell is given by

$$\cos(\Delta_0) = \frac{\dot{R}_M(0)}{\sqrt{-h_{\phi\phi}(0)h_{\sigma\sigma}(0)}}. \quad (2.31)$$

The total angle around the point  $\phi = 0$  on the shell is given by  $\delta_0 = \pi + 2\Delta_0$ ,

$$\delta_0 = 2\pi\gamma_0, \quad (2.32a)$$

$$\gamma_0 = \frac{1}{2} + \frac{1}{\pi} \arccos\left(\frac{\dot{R}_M(0)}{\sqrt{-h_{\phi\phi}(0)h_{\sigma\sigma}(0)}}\right). \quad (2.32b)$$

The associated mass of the point particle is given by

$$\mu_0 = \frac{1}{4}(1 - \gamma_0). \quad (2.33)$$

The angular deficit or excess is an artefact of the absence of circular symmetry. In the case of a circularly symmetric shell, one has  $\dot{R}_M = 0$ . As such,  $\gamma$  (2.27) and  $\gamma_0$  (2.32) are both equal to unity and  $\mu_\pi = \mu_0 = 0$ .

### 2.5. Angular periodicity in $\mathcal{V}^+$

We comment now on the periodicity of  $\theta$  in  $\mathcal{V}^+$ . *A priori*, there is no reason for  $\Theta_M$  to be  $2\pi$  periodic and we can therefore only calculate the periodicity of  $\theta$  *a posteriori*. As such,  $M$  is in general not the ADM mass parameter. One may relate the coordinates  $(t, r_+, \theta)$  to the usual BTZ coordinates via

$$\tilde{t} = \frac{t}{\beta_M}, \quad \tilde{r}_+ = \beta_M r_+, \quad \tilde{\theta} = \frac{\theta}{\beta_M}, \quad (2.34)$$

where we have introduced

$$\beta_M := \frac{1}{2\pi} (\Theta_M(\pi) - \Theta_M(-\pi)) = \frac{1}{2\pi} \int_{-\pi}^{\pi} d\phi' \frac{1}{R_M(\phi')} \sqrt{\frac{r_0^2}{\Omega^2(r_0, \phi')} - \frac{\ell^2 \dot{R}_M^2(\phi')}{R_M^2(\phi') - M\ell^2}}, \quad (2.35)$$



such that  $\tilde{\theta}$  is  $2\pi$  periodic. In these coordinates, the shell radial and angular coordinates are

$$\tilde{R}_M(\phi) = \beta_M R_M(\phi), \quad \tilde{\Theta}_M(\phi) = \frac{\Theta_M(\phi)}{\beta_M}. \quad (2.36)$$

The exterior metric is written in its usual coordinates as

$$d\tilde{s}^2 = -\tilde{g}(\tilde{r}_+)d\tilde{t}^2 + \frac{d\tilde{r}_+^2}{\tilde{g}(\tilde{r}_+)} + \tilde{r}_+^2 d\tilde{\theta}^2, \quad (2.37a)$$

$$\tilde{g}(\tilde{r}_+) = \frac{\tilde{r}_+^2}{\ell^2} - \tilde{M}, \quad (2.37b)$$

where  $\tilde{r}_+$  is defined such that a closed loop with  $\tilde{r}_+ = \tilde{R}$  has circumference  $2\pi\tilde{R}$  and

$$\tilde{M} = \beta_M^2 M = \frac{M}{(2\pi)^2} \left( \int_{-\pi}^{\pi} d\phi' \frac{1}{R_M(\phi')} \sqrt{\frac{r_0^2}{\Omega^2(r_0, \phi')} - \frac{\ell^2 \dot{R}_M^2(\phi')}{R_M^2(\phi') - M\ell^2}} \right)^2 \quad (2.38)$$

is the ADM mass. If  $M > 0$ , then (2.37) is the BTZ metric.

### 2.6. $\mathcal{A} \rightarrow 0$ limit

All three classes of metric functions listed in Table 2 reduce to the solution (2.5) in the limit  $\mathcal{A} \rightarrow 0$  with the identifications  $\pm m^2/\alpha^2 = M$ ,  $(\sigma, r, \phi) = (t, \alpha r_+, \theta/\alpha)$ , where the plus sign corresponds to Class I and the minus sign corresponds to Class II and III. In this section, we make some observations about the behaviour of the shell in this limit.

The metric function  $f(r)$  reads

$$f(r) = \frac{r^2}{\ell^2} \pm m^2, \quad (2.39)$$

where  $+m^2$  denotes the Class I solution and  $-m^2$  denotes the Class II and III solutions. In all classes, we have  $\Omega(r, \phi) \rightarrow 1$  as  $\mathcal{A} \rightarrow 0$ . The shell radial and angular coordinates reduce to

$$R_M(\phi) = R_M := \ell \sqrt{\frac{f(r_0)}{\alpha^2} + M}, \quad \Theta_M(\phi) = \frac{r_0}{R_M} \phi. \quad (2.40)$$

We note that the shell is circularly symmetric and that  $\Theta_M(\phi)$  is  $2\pi$  periodic when  $R_M = r_0$ .

The minimum value of the exterior mass parameter is given by

$$M_{\min} = -\frac{f(r_0)}{\alpha^2} \quad (2.41)$$

and as  $M \rightarrow M_{\min}$ , we have  $R_M \rightarrow 0$ . This is in contrast to the case when  $\mathcal{A} \neq 0$ , in which case  $M \rightarrow M_{\min}$  does not imply  $R_M(\phi) \rightarrow 0$ .

The ADM mass  $\tilde{M}$  is given by

$$\tilde{M} = \frac{r_0^2}{R_M^2} M \quad (2.42)$$

from (2.38). We see that  $\tilde{M} = M$  exactly when  $\Theta_M(\phi)$  is  $2\pi$  periodic (for which  $r_0 = R_M$ ).

In the  $\mathcal{A} \rightarrow 0$  limit, the radial and angular coordinates of the shell  $R_M$  and  $\Theta_M(\phi)$  are sufficiently simple that we may find the energy density and pressure of the shell explicitly.

Substituting  $R_M$  and  $\Theta_M(\phi)$  as given by (2.40) into the expressions between (2.16) and (2.23), we find

$$\rho = \frac{\sqrt{f(r_0)}}{8\pi r_0} \left( 1 - \frac{r_0}{\alpha R_M} \right), \quad (2.43a)$$

$$p = \frac{\alpha R_M}{8\pi \ell^2 \sqrt{f(r_0)}} \left( 1 - \frac{r_0}{\alpha R_M} \right). \quad (2.43b)$$

Using (2.40), we find

$$p = \frac{r_0}{\ell} \frac{\sqrt{f(r_0) + \alpha^2 M}}{f(r_0)} \rho \quad (2.44)$$

for the equation of state of the shell. The energy density and pressure of the shell will be positive provided  $\alpha R_M > r_0$ , or  $M\alpha^2 \pm m^2 > 0$ . If the exterior metric is BTZ ( $M > 0$ ) then only class II and III metrics can have shells with negative energy density.

We consider now two special cases. First, we consider  $R_M = r_0$ , when  $\Theta_M(\phi)$  is  $2\pi$  periodic and  $\widetilde{M} = M$ . Using the definition of  $R_M$  (2.40), this is the case when

$$\frac{r_0^2}{\ell^2}(\alpha^2 - 1) = M\alpha^2 \pm m^2, \quad (2.45)$$

where  $+m^2$  corresponds to Class I and  $-m^2$  corresponds to Class II and III. For  $\alpha = 1$ , we see (2.45) is satisfied for

$$M = \mp m^2. \quad (2.46)$$

In this case, the metrics in  $\mathcal{V}^+$  and  $\mathcal{V}^-$  identically agree. Furthermore, for  $\alpha = 1$  (and recalling  $R_M = r_0$ ), we see both the energy density and pressure (2.43) vanish; there is no shell. However, for  $\alpha \neq 1$ ,  $\Theta_M(\phi)$  is still  $2\pi$  periodic but with nonzero shell energy density and pressure. The energy density and pressure of the shell is positive for  $\alpha > 1$  and negative for  $0 < \alpha < 1$ .

In constructing the shell in Section 2.3, we enforced  $t = \sigma$ . As such, the time coordinates interior and exterior to the shell only agree for  $\alpha = 1$ . For  $\alpha \neq 1$ , the time coordinates do not agree and there must be a shell of stress energy sourcing this difference.

Second, we consider the extremal case  $M \rightarrow M_{\min} = -f(r_0)/\alpha^2$ . In this case, the radius  $R_M$  tends to zero, implying the pressure (2.43b)  $p \rightarrow -r_0 / (8\pi \ell^2 \sqrt{f(r_0)})$  and the energy density (2.43a) diverges:  $\rho \rightarrow -\infty$ . As  $R_M \rightarrow 0$  and  $M_{\min} < 0$ , we have by (2.42) that  $\widetilde{M}_{\min} \rightarrow -\infty$ , consistent with the infinite negative energy density sourced by the shell. This is again in contrast with the accelerated solution, whose ADM minimum mass does not diverge owing to the nonzero limit of  $R_M(\phi)$  as  $M \rightarrow M_{\min}$ .

Finally, we address the angular deficit or excess at  $\phi = \pm\pi$ , and also at  $\phi = 0$  in Class III. As  $\mathcal{A} \rightarrow 0$ , we see  $R_M(\phi)$  tends to a constant (2.40) and so  $\dot{R}_M \rightarrow 0$ . In this case, the angular deficit or excess characterised by (2.27) and (2.32) vanishes:  $\gamma, \gamma_0 \rightarrow 1$ . As such, the point particle mass (2.28) and (2.33) vanishes:  $\mu_\pi, \mu_0 \rightarrow 0$  as  $\mathcal{A} \rightarrow 0$ . This is consistent with the interpretation that the angular deficit or excess is an artefact of the lack of circular symmetry of the shell.

## 2.7. Large- $M$ limit

We consider now the leading-order asymptotic behaviour of the shell for large values of the exterior mass parameter  $M$ .

In the limit  $M \rightarrow \infty$ , the shell radius and angular coordinate as viewed from outside the shell are given by

$$R_M(\phi) \sim \ell\sqrt{M}, \quad (2.47a)$$

$$\Theta_M(\phi) \sim \frac{r_0}{\ell\sqrt{M}} \int_0^\phi d\phi' \frac{1}{\Omega(r_0, \phi')}, \quad (2.47b)$$

where we have used (2.9). The asymptotic behaviour of  $\beta_M$  (2.35) is given by

$$\beta_M \sim \frac{r_0}{2\pi\ell\sqrt{M}} \int_{-\pi}^\pi d\phi' \frac{1}{\Omega(r_0, \phi')}, \quad (2.48)$$

such that the ADM shell radius (2.36),

$$\beta_M R_M(\phi) \sim \frac{r_0}{2\pi} \int_{-\pi}^\pi d\phi' \frac{1}{\Omega(r_0, \phi')}, \quad (2.49)$$

asymptotes to a constant.

The leading-order asymptotic behaviour of the ADM mass parameter  $\widetilde{M}$  (2.38) is given by

$$\widetilde{M}_{\max} \sim \left(\frac{r_0}{2\pi\ell}\right)^2 \left(\int_{-\pi}^\pi d\phi' \frac{1}{\Omega(r_0, \phi')}\right)^2 \quad (2.50)$$

which is positive, thus implying a black hole solution. Together (2.50) and (2.10) imply that the ADM mass of the exterior spacetime is bounded both from above and below.

In the large- $M$  limit, the energy density and pressure of the shell are given by

$$\rho(\phi) \sim \frac{\sqrt{f(r_0)}}{8\pi r_0}, \quad (2.51a)$$

$$p(\phi) \sim \frac{\alpha\Omega(r_0, \phi)}{8\pi\sqrt{f(r_0)}}\sqrt{M}. \quad (2.51b)$$

As the stress energy  $\rho$  in (2.51) is positive, we can always construct a shell with a physical stress energy for the heaviest, allowable, black-hole BTZ solution. Furthermore, the energy density of the shell is evenly distributed since it is independent of the shell intrinsic coordinate  $\phi$ . However, the pressure of the constructed shell increases without bound.

To consider the point mass located at the end of the string (or strings for the Class III solution), we begin with the identity

$$\dot{R}_M(\phi) = \frac{\ell^2 f(r_0)}{\alpha^2 R_M(\phi)} \Omega(r_0, 0) \dot{\Omega}(r_0, \phi). \quad (2.52)$$

All  $M$ -dependence is found in  $R_M \sim \ell\sqrt{M}$  by (2.47). As such, the angular deficit/excess  $\gamma$  in (2.27) at  $\phi = \pm\pi$  is given by

$$\gamma \sim 1 + \frac{\ell f(r_0)}{\alpha^2 \sqrt{M}} \Omega(r_0, \pi) \dot{\Omega}(r_0, \pi). \quad (2.53)$$

The leading-order behaviour of the associated mass of the point particle is then

$$\mu_\pi \sim -\frac{\ell f(r_0)}{4\alpha^2 \sqrt{M}} \Omega(r_0, \pi) \dot{\Omega}(r_0, \pi). \quad (2.54)$$

Similarly, in the Class III spacetime, the leading-order behaviour of the mass of the point particle at  $\phi = 0$  is given by

$$\mu_0 \sim \frac{\ell f(r_0)}{4\alpha^2 \sqrt{M}} \Omega(r_0, 0) \dot{\Omega}(r_0, 0). \quad (2.55)$$

The mass of the point particle due to an angular deficit or excess therefore decays as  $M^{-1/2}$ . That the mass tends to zero for large  $M$  is consistent with the observation in Section 2.4 that the angular deficit/excess originates from the lack of circular symmetry of the shell. In the large- $M$  limit, we see that the shell radius tends to a constant (2.47) (or (2.49) in ADM coordinates). As such, the shell becomes circularly symmetric and its angular deficit or excess should vanish, along with mass of the point particle.

We now proceed to analyse the properties of the shell for each class in Table 2.

### 3. Class I<sub>pulled</sub>: Particle pulled by a string

In this section, we consider the Class I<sub>pulled</sub> C-metric solution, describing a particle pulled by a string. In polar coordinates  $(\sigma, r, \phi)$ , the metric reads

$$ds_-^2 = \frac{1}{\Omega^2(r, \phi)} \left( -\frac{f(r)}{\alpha^2} d\sigma^2 + \frac{dr^2}{f(r)} + r^2 d\phi^2 \right), \quad (3.1a)$$

$$f(r) = \frac{r^2}{\ell^2} + m^2(1 - \mathcal{A}^2 r^2), \quad (3.1b)$$

$$\Omega(r, \phi) = 1 + \mathcal{A}r \cos(m\phi), \quad (3.1c)$$

where  $0 < m < 1$ . The tension of the string is given by

$$\tau_\pi = \frac{1}{4\pi} m \mathcal{A} \sin(m\pi). \quad (3.2)$$

We demonstrate now why this metric may be interpreted as describing the geometry around a point particle. This may be clearly seen by considering the spacetime near  $r = 0$ . To leading order we have

$$ds^2 = -d\tilde{t}^2 + d\tilde{r}^2 + \tilde{r}^2 d\tilde{\phi}^2, \quad (3.3)$$

where  $\tilde{t} = m\sigma/\alpha$ ,  $\tilde{r} = r/m$ , and  $\tilde{\phi} = m\phi$ . This is  $(2+1)$ -dimensional Minkowski spacetime but with an angular coordinate  $\tilde{\phi}$  with a periodicity of  $2m\pi < 2\pi$  — the spacetime has an angular deficit. It is this angular deficit that allows us to interpret the Class I solution as a point particle as an angular deficit has an associated mass [35],

$$m_{\text{ad}} = \frac{1}{4}(1 - m). \quad (3.4)$$

We see that as  $m \rightarrow 1$ ,  $\tilde{\phi}$  becomes  $2\pi$  periodic and the mass of the point particle vanishes.

The spacetime (3.1) has a conformal boundary at

$$r_{\text{conf}} = -\frac{1}{\mathcal{A} \cos(m\phi)}. \quad (3.5)$$

Taking the limit  $\mathcal{A} \rightarrow 0$  and identifying  $m^2 = \alpha^2 M$  with  $M < 0$ , one recovers the geometry of a non-rotating point particle (2.5) in coordinates  $(\sigma, r, \phi) = (t, \alpha r_+, \theta/\alpha)$ . We note that the Class I solution can be continuously deformed into Class II by letting  $m^2 \rightarrow -m^2$  with  $\mathcal{A}$  fixed.

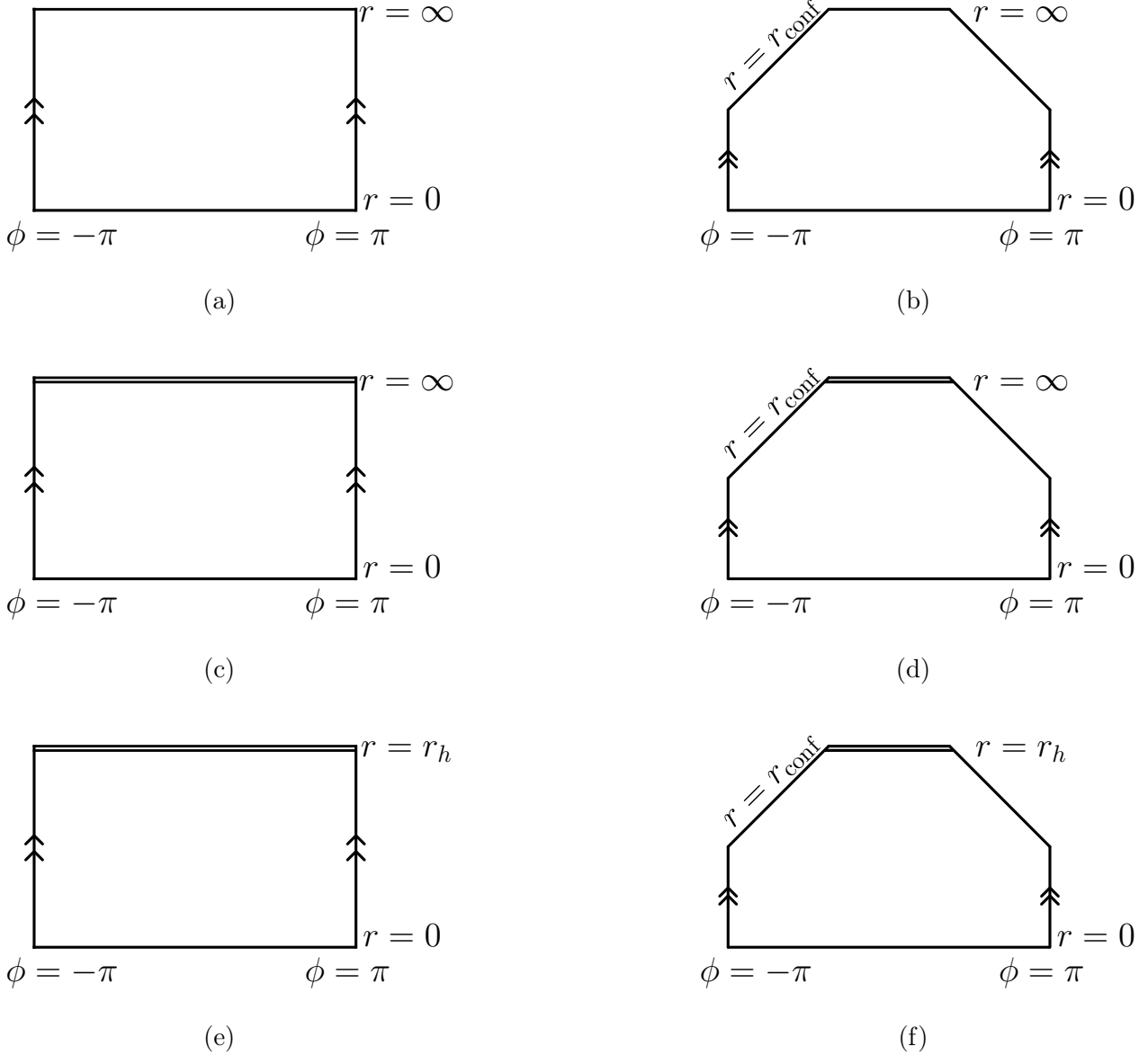


Figure 1: Constant time slice of the Class  $I_{\text{pulled}}$  solution describing a particle being pulled by a string. **(a)** Slow acceleration with  $m \leq \frac{1}{2}$ . **(b)** Slow acceleration with  $m > \frac{1}{2}$ . **(c)** Saturated acceleration with  $m \leq \frac{1}{2}$ . **(d)** Saturated acceleration with  $m > \frac{1}{2}$ . **(e)** Rapid acceleration with  $m \leq \frac{1}{2}$ . **(f)** Rapid acceleration with  $m > \frac{1}{2}$ . Double lines in **(c)**-**(f)** represent a Killing horizon.

This geometry exhibits three different phases of acceleration, dubbed *slow* ( $m^2 \mathcal{A}^2 \ell^2 < 1$ ), *saturated* ( $m^2 \mathcal{A}^2 \ell^2 = 1$ ), and *rapid* ( $m^2 \mathcal{A}^2 \ell^2 > 1$ ). In the slow acceleration regime, the geometry has no horizons; whereas for  $m^2 \mathcal{A}^2 \ell^2 \geq 1$ , there is a Killing horizon at

$$r_h = \frac{m\ell}{\sqrt{m^2 \mathcal{A}^2 \ell^2 - 1}}, \quad (3.6)$$

referred to as the acceleration horizon. The geometry of the three phases is depicted in Figure 1.

For all phases of the acceleration, the minimum value of the exterior mass parameter  $M$  (2.10) is given by

$$M_{\min} = \frac{f(r_0) (m^2 \mathcal{A}^2 \ell^2 \sin^2(m\phi_*) - 1)}{\alpha^2 (1 + \mathcal{A}r_0 \cos(m\phi_*))^2}, \quad (3.7a)$$

$$\phi_* = \begin{cases} 0 & \text{for } m \leq \frac{1}{\mathcal{A}\ell} \sqrt{\frac{\mathcal{A}r_0}{1+\mathcal{A}r_0}}, \\ \min \left\{ \frac{1}{m} \arccos \left( \frac{(1-m^2\mathcal{A}^2\ell^2)\mathcal{A}r_0}{m^2\mathcal{A}^2\ell^2} \right), \pi \right\} & \text{for } m > \frac{1}{\mathcal{A}\ell} \sqrt{\frac{\mathcal{A}r_0}{1+\mathcal{A}r_0}}. \end{cases} \quad (3.7b)$$

We make three observations. First, for  $\phi_* = \frac{1}{m} \arccos \left( \frac{(1-m^2\mathcal{A}^2\ell^2)\mathcal{A}r_0}{m^2\mathcal{A}^2\ell^2} \right)$ , we may simplify (3.7)

$$M_{\min} = -\frac{m^2}{\alpha^2} (1 - m^2\mathcal{A}^2\ell^2). \quad (3.8)$$

Second, since  $\mathcal{A}r_0/(1 + \mathcal{A}r_0) \in (0, 1)$ , we may simplify (3.7) for saturated accelerations,

$$M_{\min} = -\frac{f(r_0)}{\alpha^2} \frac{\cos^2(m\phi_*)}{(1 + \mathcal{A}r_0 \cos(m\phi_*))^2}, \quad (3.9a)$$

$$\phi_* = \min \left\{ \frac{\pi}{2m}, \pi \right\}, \quad (3.9b)$$

in which case we have  $M_{\min} = 0$  for  $1/2 < m < 1$ . Otherwise, for  $0 < m \leq 1/2$ , we have  $M_{\min} < 0$ . Finally, for rapid accelerations ( $m\mathcal{A}\ell > 1$ ) (3.7) simplifies to

$$\phi_* = \min \left\{ \frac{1}{m} \arccos \left( \frac{(1 - m^2\mathcal{A}^2\ell^2)\mathcal{A}r_0}{m^2\mathcal{A}^2\ell^2} \right), \pi \right\} \quad (3.10)$$

using again  $\mathcal{A}r_0/(1 + \mathcal{A}r_0) \in (0, 1)$ .

The shell radius  $R_M(\phi)$  (2.9a) has the following asymptotic behaviour

$$R_M(\phi) \sim \ell \left( \sqrt{\frac{f(r_0)}{\alpha^2(1 + \mathcal{A}r_0)^2} + M} \right) + \frac{\mathcal{A}\ell m^2 r_0 f(r_0)}{2\alpha^2(1 + \mathcal{A}r_0)^3} \frac{1}{\sqrt{\frac{f(r_0)}{\alpha^2(1 + \mathcal{A}r_0)^2} + M}} \phi^2 + \mathcal{O}(\phi^4) \quad (3.11)$$

around  $\phi = 0$ . We see that the leading term is a strictly increasing function of  $M$ , whereas the coefficient of the quadratic term is a strictly decreasing function of  $M$ . As  $M \rightarrow M_{\min}$ , we see the leading term attains its minimum value, whereas the coefficient of the quadratic term attains its maximum value.

### 3.1. Slow acceleration

We consider first the slow acceleration regime,  $m^2\mathcal{A}^2\ell^2 < 1$ . In this regime, (3.7) implies  $M_{\min} < 0$ .

In Figure 2 **(a)** and **(b)**, we plot the radial coordinate  $\tilde{R}_M$  (2.36) and angular coordinate  $\tilde{\Theta}_M$  (2.36) as functions of the shell's intrinsic coordinate  $\phi$ . For small values of  $M$ , the shell resembles a cardioid, pinched outwards near the string at  $\phi = \pi$  and developing a more pronounced cuspidal shape at  $\phi = 0$  as  $\tilde{M} \rightarrow \tilde{M}_{\min}$ . We see from (3.11) that the first derivative exists at  $\phi = 0$  and hence there is no sharp cusp. The angular coordinate  $\Theta_M$  increasingly deviates from linearity as  $M \rightarrow M_{\min}$ . As  $\tilde{M}$  gets larger, the shell becomes less deformed, approaching near-circular teardrop shape as  $\tilde{M} \rightarrow \tilde{M}_{\max}$ , as anticipated by (2.47). The dashed line indicates the string, which extends from the point particle (centred at the origin in these coordinates) out to the shell.

Both shell density and pressure are maximised at the cusp, being highly concentrated there as  $\tilde{M} \rightarrow \tilde{M}_{\min}$ , shown in Figure 2 **(c)** and Figure 2 **(d)**. As the shell approaches the string, both decrease super-exponentially rapidly, but do not vanish. These two maxima are consistent with our modelling of the stress energy as a perfect fluid; the shell is being pulled by the string

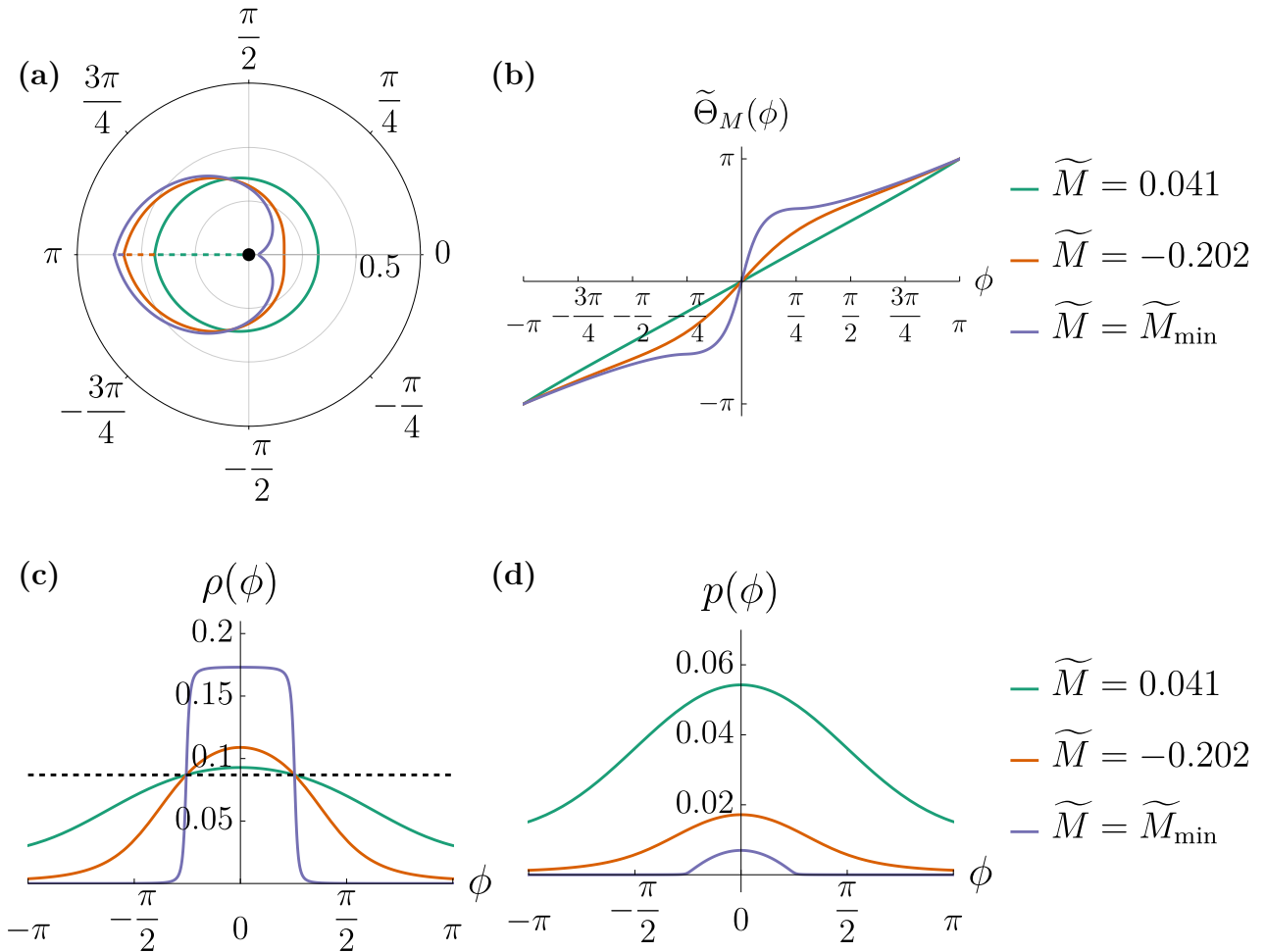


Figure 2: Class  $I_{\text{pulled}}$  (slow phase) for  $r_0 = 0.4$ ,  $m = 0.8$ ,  $\mathcal{A} = 0.6$ ,  $\alpha = 0.25$ ,  $\ell = 1$ , with  $\tilde{M}_{\min} \approx -0.283$ , and  $\tilde{M}_{\max} \approx 0.149$ . (a) Polar plot of shell radius  $\tilde{R}_M$  (2.36) over  $\phi \in (-\pi, \pi)$  for varying values of  $\tilde{M}$ ; dashed line is the string and black dot represents the point particle. (b) Shell angular coordinate  $\tilde{\Theta}_M$  (2.36) for varying values of  $\tilde{M}$ . (c) Energy density of the shell as a function of the shell's intrinsic spatial coordinate  $\phi$  for varying values of  $\tilde{M}$ . Black dashed line at asymptotic value as  $\tilde{M} \rightarrow \tilde{M}_{\max}$ . (d) Pressure of the shell as a function of the shell's intrinsic coordinate  $\phi$  for varying values of  $\tilde{M}$ .

at  $\phi = \pm\pi$ , so one would expect the fluid to “pool” opposite the string, at  $\phi = 0$ . As the ADM mass  $\tilde{M}$  gets larger, the pressure generally increases, but becomes greater on the part of the shell farthest from the string. It is straightforward to check that the stress energy of the shell satisfies the strong energy condition. As  $\tilde{M} \rightarrow \tilde{M}_{\min}$ , the stress energy of the shell is positive but decays faster than exponentially. The behaviour of the stress energy as  $\tilde{M} \rightarrow \tilde{M}_{\max}$  is given by (2.51); the energy density  $\rho$  tends to a constant, whereas the pressure still depends on  $\phi$ .

### 3.2. Saturated acceleration

In the saturated acceleration phase,  $m^2 \mathcal{A}^2 \ell^2 = 1$ , we find that the shell has features similar to the slow acceleration case, the most notable distinction being the absence of a cusp as  $\tilde{M} \rightarrow \tilde{M}_{\min}$ . We remark that  $\tilde{M}_{\min} = 0$ ; hence the  $\tilde{M} = \tilde{M}_{\min}$  plot depicts a shell with an exterior geometry of Torricelli's trumpet.

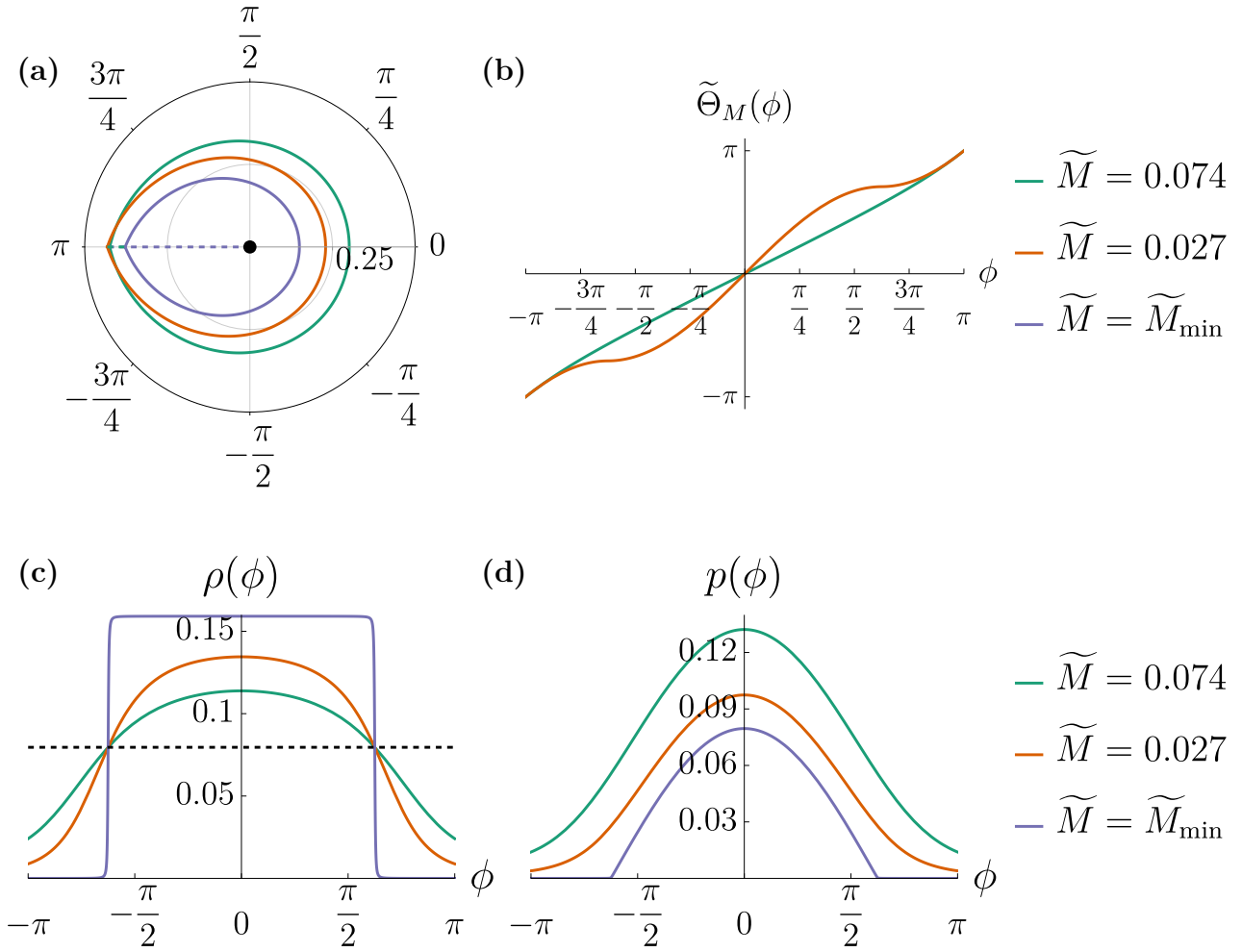


Figure 3: Class  $I_{\text{pulled}}$  (saturated phase), for  $r_0 = 0.4$ ,  $m = 0.8$ ,  $\mathcal{A} = 1.25$ ,  $\alpha = 0.25$ ,  $\ell = 1$ , with  $\tilde{M}_{\min} = 0$ , and  $\tilde{M}_{\max} \approx 0.151$ . **(a)** Polar plot of shell radius  $\tilde{R}_M$  (2.36) over  $\phi \in (-\pi, \pi)$  for varying values of  $\tilde{M}$ ; dashed line indicates the string and black dot represents the point particle. **(b)** Shell angular coordinate  $\tilde{\Theta}_M$  (2.36) for varying values of  $\tilde{M}$ . **(c)** Energy density of the shell as a function of the shell's intrinsic spatial coordinate  $\phi$  for varying values of  $\tilde{M}$ . Black dashed line at asymptotic value as  $\tilde{M} \rightarrow \tilde{M}_{\max}$ . **(d)** Pressure of the shell as a function of the shell's intrinsic coordinate  $\phi$  for varying values of  $\tilde{M}$ .

We plot the various results in Figure 3 (a) to (d). We see from Figure 3 (a) that, in contrast to the slow acceleration phase, the shell remains regular near  $\phi = 0$  as  $\tilde{M} \rightarrow \tilde{M}_{\min}$ , maintaining a teardrop shape, pinched at the string  $\phi = \pi$ , for all values of  $\tilde{M}$ . The angular coordinate (2.36) grows monotonically with  $\phi$  (Figure 3 (b)), but with notably reduced non-linear behaviour for small  $\tilde{M}$ . The density is notably larger on the part of the shell that is away from its pinch (Figure 3 (c)). The pressure, shown in Figure 3 (d), is always maximal opposite the pinch. This is again consistent with our modelling of the stress energy as a perfect fluid. Again, the stress energy of the shell satisfies the strong energy condition. As  $\tilde{M} \rightarrow \tilde{M}_{\min}$ , the stress energy of the shell is positive but decays faster than exponentially. The behaviour of the stress energy as  $\tilde{M} \rightarrow \tilde{M}_{\max}$  is given by (2.51); the energy density  $\rho$  tends to a constant, whereas the pressure still depends on  $\phi$ .



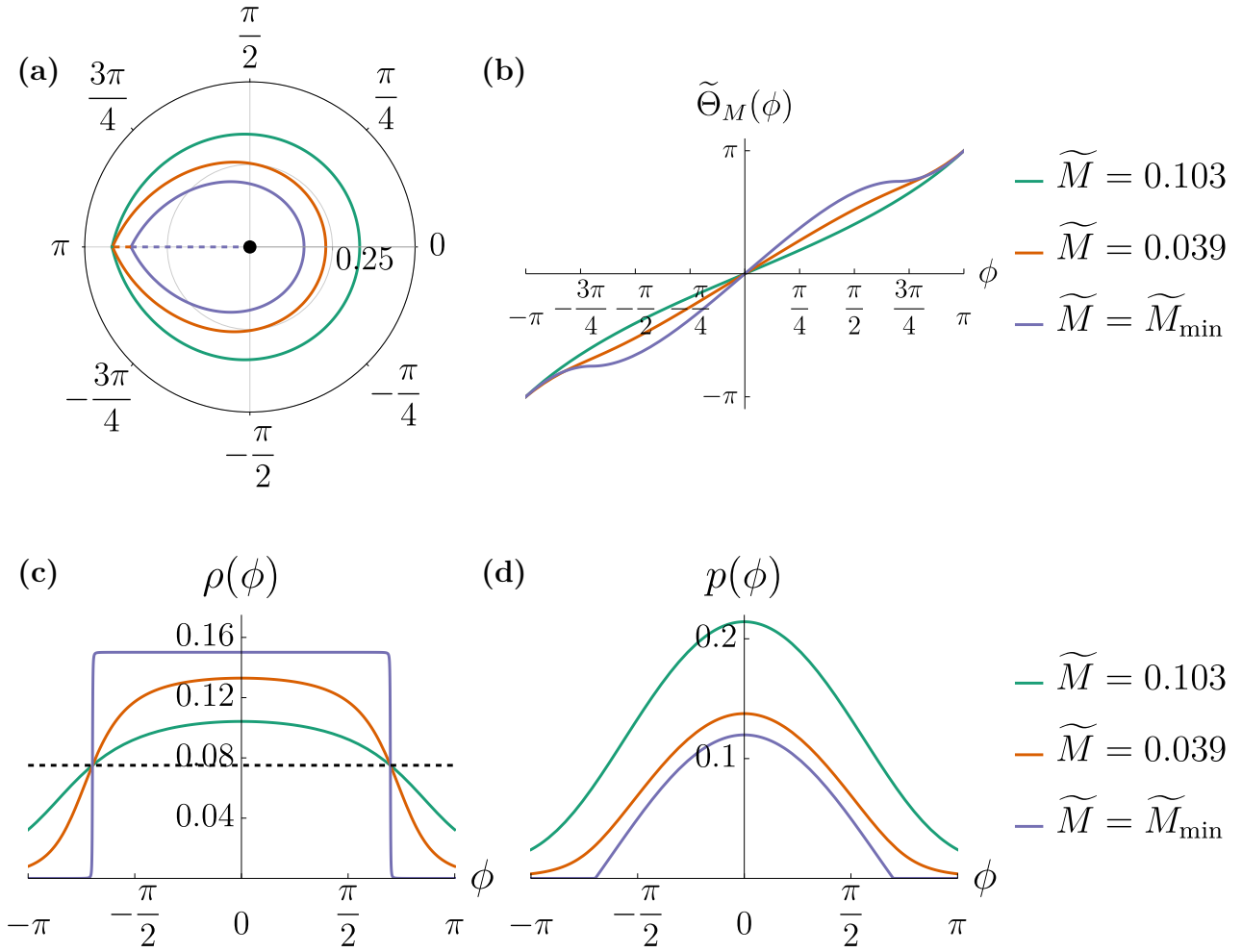


Figure 4: Class I<sub>pulled</sub> (rapid phase) for  $r_0 = 0.4$ ,  $m = 0.8$ ,  $\mathcal{A} = 1.5$ ,  $\alpha = 0.25$ ,  $\ell = 1$ ,  $r_h \approx 1.206$ , with  $\widetilde{M}_{\min} \approx 0.015$ , and  $\widetilde{M}_{\max} \approx 0.157$ . **(a)** Polar plot of shell radius  $\widetilde{R}_M$  (2.36) over  $\phi \in (-\pi, \pi)$  for varying values of  $\widetilde{M}$ ; dashed line indicates the string and black dot represents the point particle. **(b)** Shell angular coordinate  $\widetilde{\Theta}_M$  (2.36) for varying values of  $\widetilde{M}$ . **(c)** Energy density of the shell as a function of the shell's intrinsic spatial coordinate  $\phi$  for varying values of  $\widetilde{M}$ . Black dashed line at asymptotic value as  $\widetilde{M} \rightarrow \widetilde{M}_{\max}$ . **(d)** Pressure of the shell as a function of the shell's intrinsic coordinate  $\phi$  for varying values of  $\widetilde{M}$ .

### 3.3. Rapid acceleration

The rapid acceleration phase,  $m^2 \mathcal{A}^2 \ell^2 > 1$ , has features quite similar to the saturated phase. Results are shown in Figure 4 **(a)** to **(d)**.

The teardrop shape of the shell is still present, and the density and pressure are still maximised opposite the pinch. The most notable distinction is that the high-density region of the shell extends well past half its circumference, shown in Figure 4 **(c)**. The strong energy condition is still respected. As  $\widetilde{M} \rightarrow \widetilde{M}_{\min}$ , the stress energy of the shell is positive but decays faster than exponentially. The behaviour of the stress energy as  $\widetilde{M} \rightarrow \widetilde{M}_{\max}$  is given by (2.51); the energy density  $\rho$  tends to a constant, whereas the pressure still depends on  $\phi$ .

4. Class  $I_{\text{pushed}}$ : Particle pushed by a strut

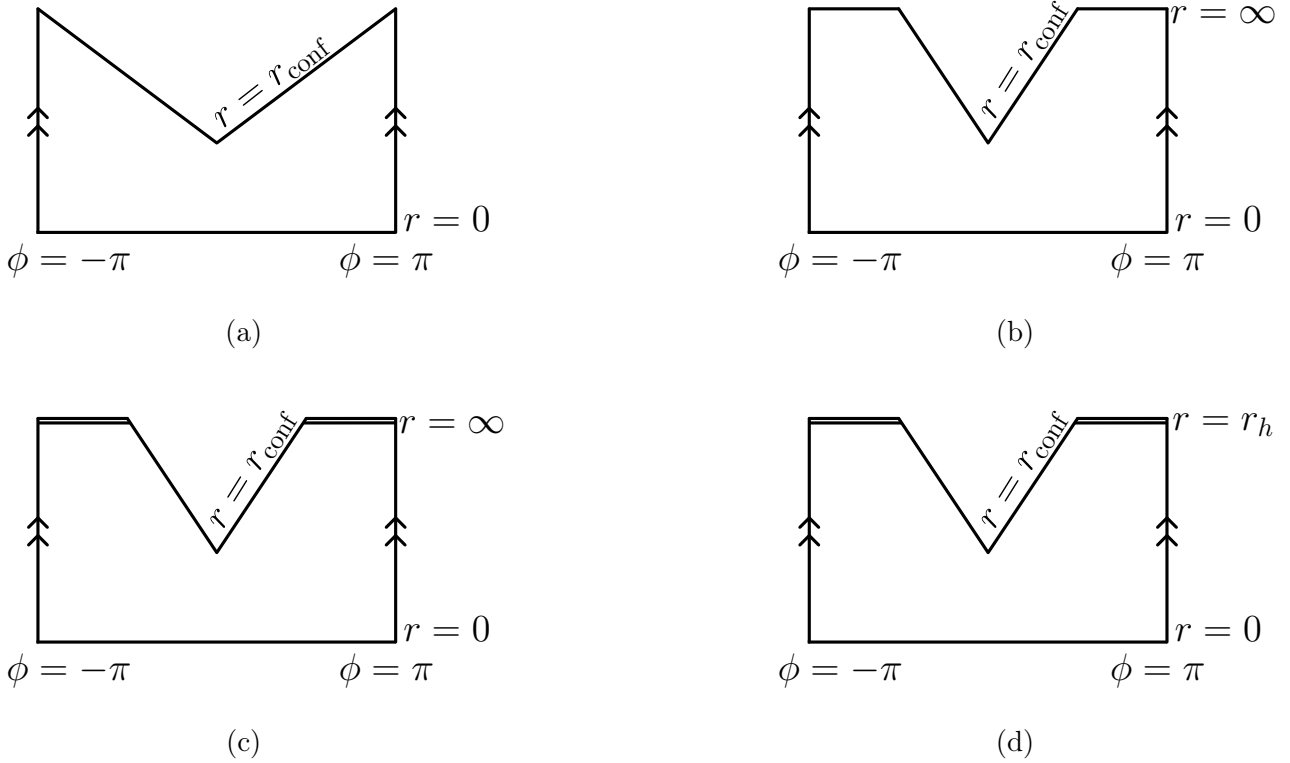


Figure 5: Constant time slice of the Class  $I_{\text{pushed}}$  solution describing a particle being pushed by a strut. **(a)** Slow and saturated acceleration regimes with  $m \leq \frac{1}{2}$  and rapid acceleration regime with  $m\mathcal{A}\ell \sin(m\pi) \leq 1$ . **(b)** Slow acceleration with  $m > \frac{1}{2}$ . **(c)** Saturated acceleration with  $m > \frac{1}{2}$ . **(d)** Rapid acceleration with  $m\mathcal{A}\ell \sin(m\pi) > 1$ . Double lines in **(c)** and **(d)** represent a Killing horizon.

We consider now the Class  $I_{\text{pushed}}$  metric solution describing a particle pushed by a strut. The metric of this spacetime is found by mapping  $\mathcal{A} \rightarrow -\mathcal{A}$  in (3.1),

$$ds^2 = \frac{1}{\Omega^2(r, \phi)} \left( -\frac{f(r)}{\alpha^2} d\sigma^2 + \frac{dr^2}{f(r)} + r^2 d\phi \right), \quad (4.1a)$$

$$f(r) = \frac{r^2}{\ell^2} + m^2 (1 - \mathcal{A}^2 r^2), \quad (4.1b)$$

$$\Omega(r, \phi) = 1 - \mathcal{A}r \cos(m\phi). \quad (4.1c)$$

The tension of the strut is given by

$$\tau_\pi = -\frac{1}{4\pi} m\mathcal{A} \sin(m\pi). \quad (4.2)$$

As in the Class  $I_{\text{pulled}}$  solution in Section 3, the Class  $I_{\text{pushed}}$  spacetime also admits slow, saturated, and rapid acceleration regimes depending on whether  $m^2\mathcal{A}^2\ell^2$  is greater than, less than, or equal to unity. For  $m^2\mathcal{A}^2\ell^2 \geq 1$ , there is a Killing horizon at

$$r_h = \frac{m\ell}{\sqrt{m^2\mathcal{A}^2\ell^2 - 1}}. \quad (4.3)$$

The geometry of the three phases of acceleration is depicted in Figure 5.

We interpret the Class  $I_{\text{pushed}}$  geometry as a point particle owing to the angular deficit in the metric (4.1). This angular deficit has the same associated mass as the Class  $I_{\text{pulled}}$  solution and is given by (3.4).

For all phases of acceleration, the minimum value of the exterior mass parameter is given by

$$M_{\min} = \frac{f(r_0)}{\alpha^2} \frac{(m^2 \mathcal{A}^2 \ell^2 \sin^2(m\phi_*) - 1)}{(1 - \mathcal{A}r_0 \cos(m\phi_*))^2}, \quad (4.4a)$$

$$\phi_* = \min \left\{ \frac{1}{m} \arccos \left( \frac{(m^2 \mathcal{A}^2 \ell^2 - 1)\mathcal{A}r_0}{m^2 \mathcal{A}^2 \ell^2} \right), \pi \right\} \quad (4.4b)$$

where

$$M_{\min} = -\frac{m^2}{\alpha^2} (1 - m^2 \mathcal{A}^2 \ell^2). \quad (4.5)$$

if  $\phi_* < \pi$ .

#### 4.1. Slow acceleration

We consider first the slow acceleration regime,  $m^2 \mathcal{A}^2 \ell^2 < 1$ . In this regime, (4.4) implies that  $M_{\min} < 0$ .

In Figure 6 **(a)** and **(b)**, we plot the radial coordinate  $\tilde{R}_M$  (2.9a) and angular coordinate  $\tilde{\Theta}_M$  (2.9b) as functions of the shell's intrinsic coordinate  $\phi$ . For small values of  $M$ , the shell again resembles a cardioid, but with a cusp now at the strut  $\phi = \pi$ . In contrast to the cuspidal shape in the Class  $I_{\text{pulled}}$  solution, this is a true cusp in the sense that the first derivatives at  $\phi = \pm\pi$  do not agree. The cusp becomes more pronounced as  $M \rightarrow M_{\min}$ . The angular coordinate  $\tilde{\Theta}_M$  has strongest deviations from linearity as  $M \rightarrow M_{\min}$ . As the ADM mass  $\tilde{M}$  gets larger, the shell becomes less deformed and approaches a circular shape as  $\tilde{M} \rightarrow \tilde{M}_{\max}$ . The dashed line indicates the strut extending from the point particle out to the shell.

We find that the shell density and pressure are both maximised at the strut at  $\phi = \pi$  pushing the point particle, being extremely concentrated there as  $\tilde{M} \rightarrow \tilde{M}_{\min}$ , shown in Figure 6 **(c)** and **(d)**. As before, these two maxima are consistent with our modelling of the stress energy as a perfect fluid; since the shell is being pushed by the strut at  $\phi = \pm\pi$ , we expect the perfect fluid to “pool” at the location of strut at  $\phi = \pm\pi$ . As  $\tilde{M} \rightarrow \tilde{M}_{\min}$ , the energy density of the shell is almost entirely localised where the strut meets the shell. The pressure of the shell increases as the ADM mass  $\tilde{M}$  get larger. This shell also satisfies the strong energy condition. As  $\tilde{M} \rightarrow \tilde{M}_{\min}$ , the stress energy of the shell is positive but decays faster than exponentially. The behaviour of the stress energy as  $\tilde{M} \rightarrow \tilde{M}_{\max}$  is given by (2.51); the energy density  $\rho$  tends to a constant, whereas the pressure still depends on  $\phi$ .

#### 4.2. Saturated acceleration

In the saturated acceleration phase,  $m^2 \mathcal{A}^2 \ell^2 = 1$ , we find that the shell has features similar to the slow acceleration case. A noticeable difference is the decreased prominence of the cusp as the shell meets the strut. We remark that  $\tilde{M}_{\min} = 0$ ; hence the  $\tilde{M} = \tilde{M}_{\min}$  plot depicts a shell with an exterior geometry of Torricelli's trumpet.

We plot the shell coordinates and stress energy in Figure 7 **(a)** to **(d)**. We see from Figure 7 that all shells are regular near  $\phi = 0$ . The angular coordinate  $\tilde{\Theta}_M$  (2.36) grows monotonically

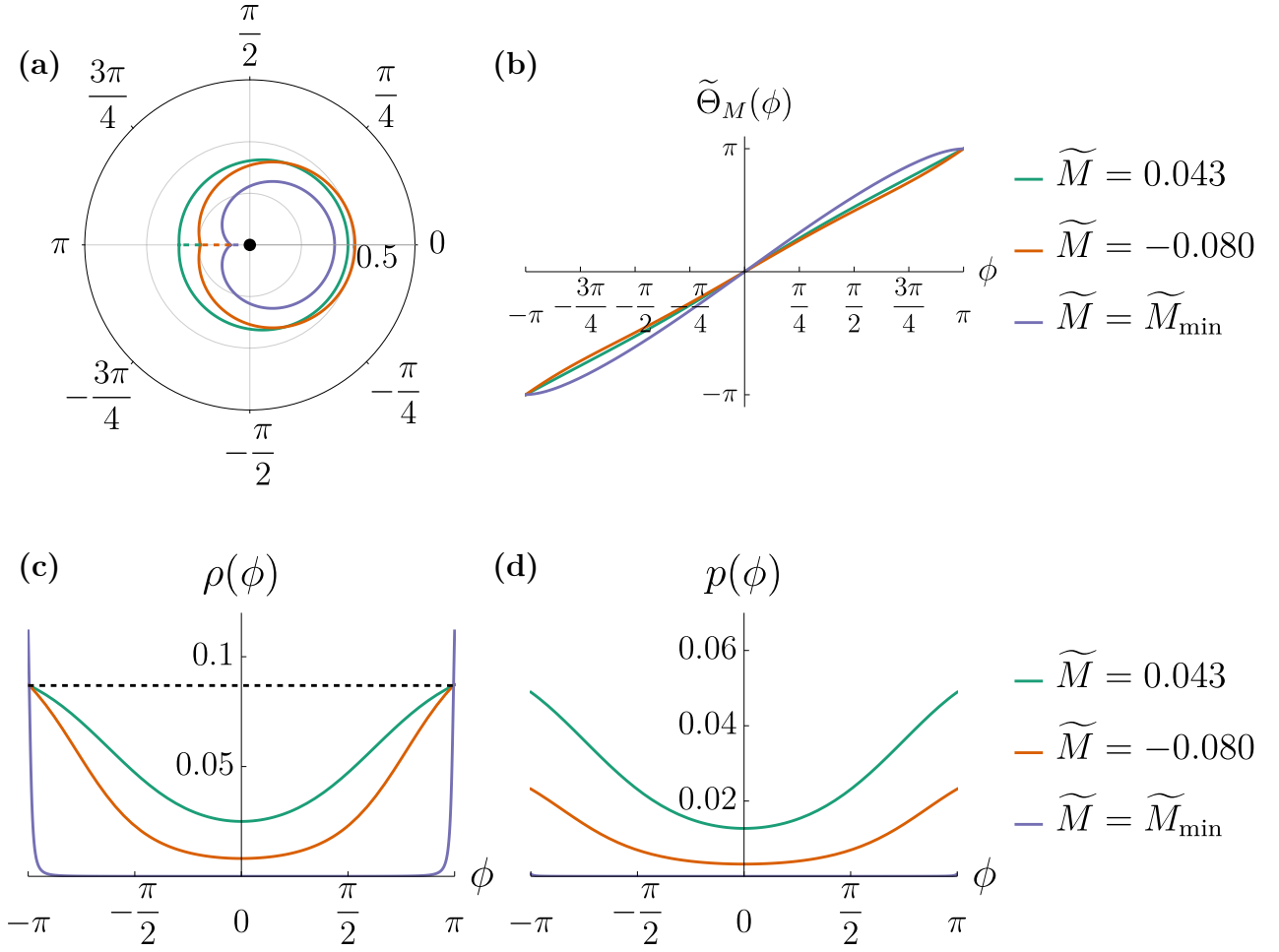


Figure 6: Class  $I_{\text{pushed}}$  (slow phase) for  $r_0 = 0.4$ ,  $m = 0.8$ ,  $\mathcal{A} = 0.6$ ,  $\alpha = 0.25$ ,  $\ell = 1$ , with  $\tilde{M}_{\min} \approx -0.100$ , and  $\tilde{M}_{\max} \approx 0.188$ . **(a)** Polar plot of shell radius  $\tilde{R}_M$  (2.36) over  $\phi \in (-\pi, \pi)$  for varying values of  $\tilde{M}$ ; dashed line indicates the strut and black dot represents the point particle. **(b)** Shell angular coordinate  $\tilde{\Theta}_M$  (2.36) for varying values of  $\tilde{M}$ . **(c)** Energy density of the shell as a function of the shell's intrinsic spatial coordinate  $\phi$  for varying values of  $\tilde{M}$ . Black dashed line at asymptotic value as  $\tilde{M} \rightarrow \tilde{M}_{\max}$ . **(d)** Pressure of the shell as a function of the shell's intrinsic coordinate  $\phi$  for varying values of  $\tilde{M}$ .

with  $\phi$  (Figure 7 (b)), but with noticeable non-linear behaviour in comparison to the slow acceleration regime. This non-linearity is emphasised for small  $\tilde{M}$ . As shown in Figure 7 (c) and (d), the energy density and pressure are concentrated on the part of the shell closest to the strut, again consistent with our modelling of the stress energy as a perfect fluid. As  $\tilde{M} \rightarrow \tilde{M}_{\min}$ , the energy density behaves like a bump function, with negligible energy density opposite the cusp. Again, the stress energy of the shell satisfies the strong energy condition. As  $\tilde{M} \rightarrow \tilde{M}_{\min}$ , the stress energy of the shell is positive but decays faster than exponentially. The behaviour of the stress energy as  $\tilde{M} \rightarrow \tilde{M}_{\max}$  is given by (2.51); the energy density  $\rho$  tends to a constant, whereas the pressure still depends on  $\phi$ .

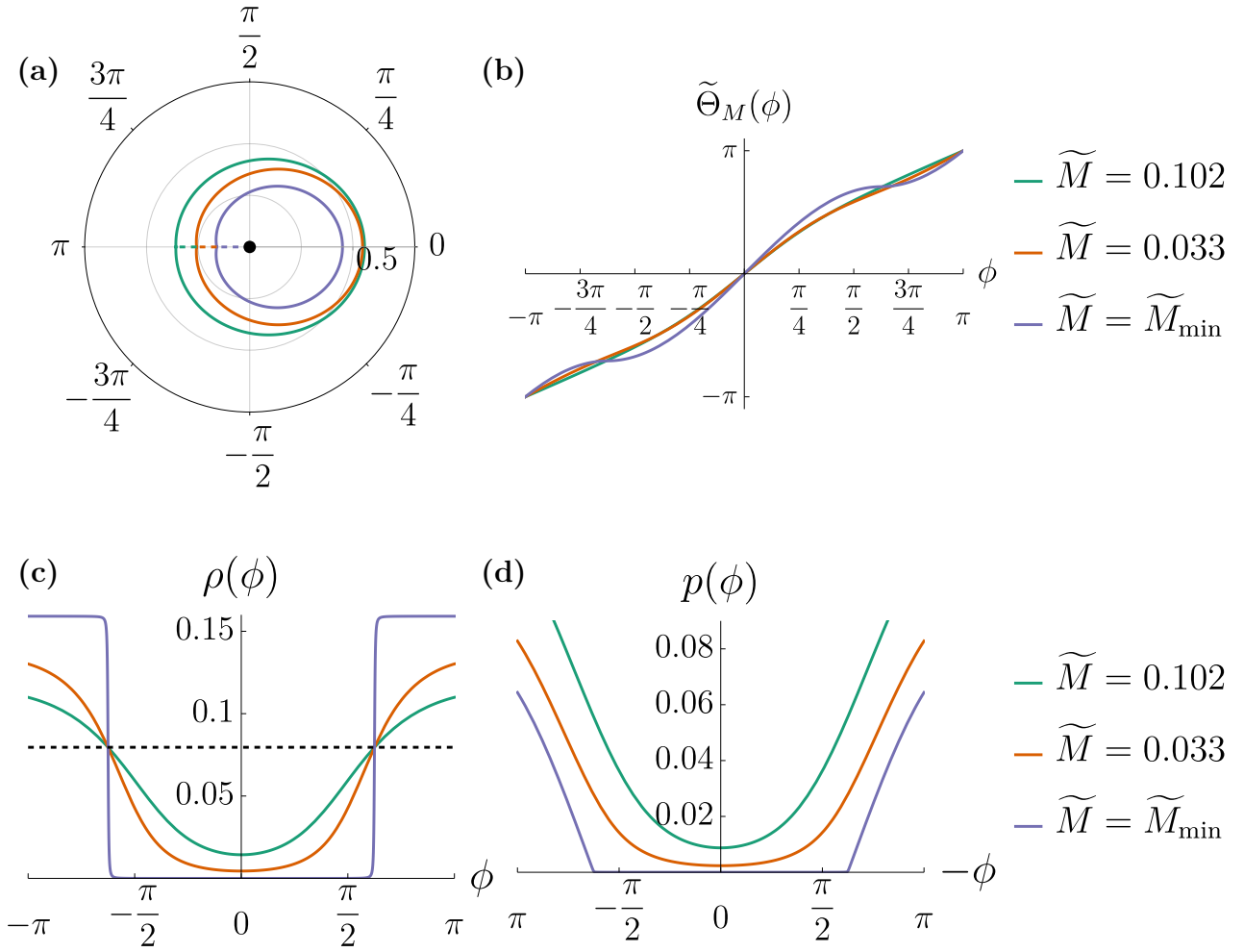


Figure 7: Class  $I_{\text{pushed}}$  (saturated phase) for  $r_0 = 0.4$ ,  $m = 0.8$ ,  $\mathcal{A} = 1.25$ ,  $\alpha = 0.25$ ,  $\ell = 1$  with  $\tilde{M}_{\min} = 0$ , and  $\tilde{M}_{\max} \approx 0.258$ . **(a)** Polar plot of shell radius  $\tilde{R}_M$  (2.36) over  $\phi \in (-\pi, \pi)$  for varying values of  $\tilde{M}$ ; dashed line indicates the strut and black dot represents the point particle. **(b)** Shell angular coordinate  $\tilde{\Theta}_M$  (2.36) for varying values of  $\tilde{M}$ . **(c)** Energy density of the shell as a function of the shell's intrinsic spatial coordinate  $\phi$  for varying values of  $\tilde{M}$ . Black dashed line at asymptotic value as  $\tilde{M} \rightarrow \tilde{M}_{\max}$ . **(d)** Pressure of the shell as a function of the shell's intrinsic coordinate  $\phi$  for varying values of  $\tilde{M}$ .

#### 4.3. Rapid acceleration

As in Class  $I_{\text{pulled}}$ , the rapid acceleration phase,  $m^2 \mathcal{A}^2 \ell^2 > 1$ , has features quite similar to the saturated phase. We show results in Figure 8 **(a)** to **(d)**.

In this phase of acceleration, the shells have a more pronounced elliptical shape, becoming more prominent as  $\tilde{M} \rightarrow \tilde{M}_{\max}$ , shown in Figure 8 **(a)**. The angular coordinate is highly nonlinear for all considered masses, owing to the elliptical shape (Figure 8 **(b)**). The high-energy density region of the shell extends almost to the arc from  $\phi = -\pi/2$  to  $\phi = \pi/2$  (Figure 8 **(c)**). The strong energy condition is also still respected. As  $\tilde{M} \rightarrow \tilde{M}_{\min}$ , the stress energy of the shell is positive but decays faster than exponentially. The behaviour of the stress energy as  $\tilde{M} \rightarrow \tilde{M}_{\max}$  is given by (2.51); the energy density  $\rho$  tends to a constant, whereas the pressure still depends on  $\phi$ .

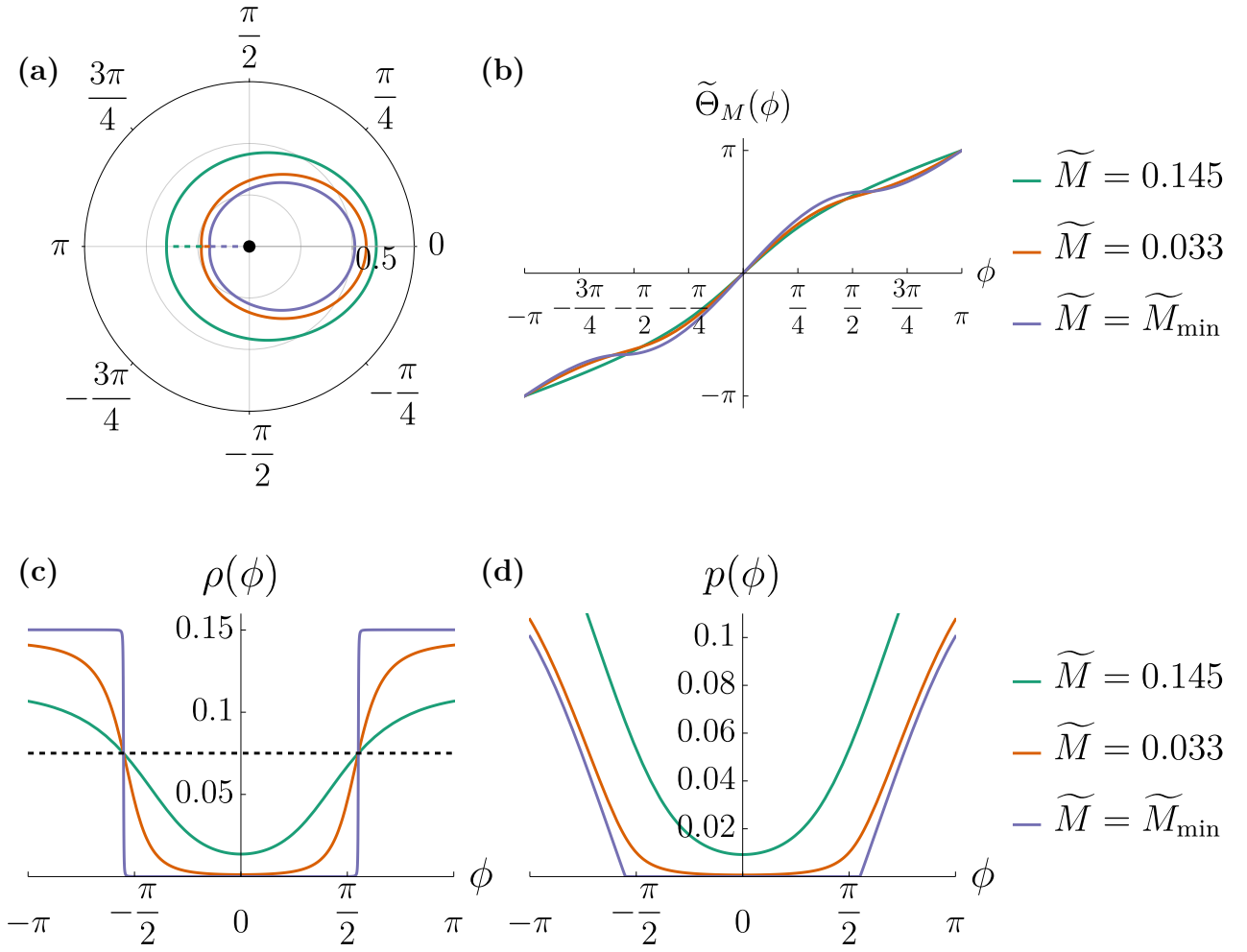


Figure 8: Class  $I_{\text{pushed}}$  (rapid phase) for  $r_0 = 0.4$ ,  $m = 0.8$ ,  $\mathcal{A} = 1.5$ ,  $\alpha = 0.25$ ,  $\ell = 1$ ,  $r_h \approx 0.019$  with  $\tilde{M}_{\min} \approx 0.015$ , and  $\tilde{M}_{\max} \approx 0.315$ . (a) Polar plot of shell radius  $\tilde{R}_M$  (2.36) over  $\phi \in (-\pi, \pi)$  for varying values of  $\tilde{M}$ ; dashed line indicates the strut and black dot represents the point particle. (b) Shell angular coordinate  $\tilde{\Theta}_M$  (2.36) for varying values of  $\tilde{M}$ . (c) Energy density of the shell as a function of the shell's intrinsic spatial coordinate  $\phi$  for varying values of  $\tilde{M}$ . Black dashed line at asymptotic value as  $\tilde{M} \rightarrow \tilde{M}_{\max}$ . (d) Pressure of the shell as a function of the shell's intrinsic coordinate  $\phi$  for varying values of  $\tilde{M}$ .

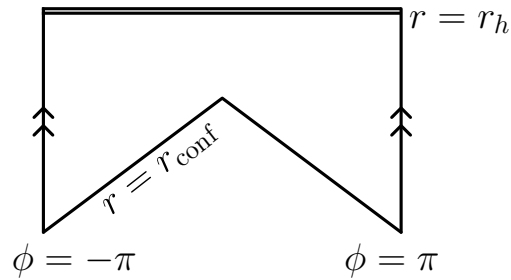


Figure 9: Constant time slice of the Class  $I_C$  solution. Double line represents a Killing horizon.

4.4. Class  $I_C$ 

We consider now the Class  $I_C$  solution, describing a black hole being pulled by a string, first described in [24]. This solution is a subregion within the parameter space of the rapid acceleration phase of the Class  $I_{\text{pushed}}$  solution.

A necessary requirement for this solution is  $0 < m < 1/2$ . Combined with the rapid acceleration phase, we require also  $\mathcal{A}\ell > 2$ . Because of this, the Class  $I_C$  black hole solution is disconnected from the non-accelerating BTZ solution given by the limit  $\mathcal{A} \rightarrow 0$ .

The geometry of the Class  $I_C$  spacetime is described by the metric

$$ds_-^2 = \frac{1}{\Omega^2(r, \phi)} \left( -\frac{f(r)}{\alpha^2} d\sigma^2 + \frac{dr^2}{f(r)} + r^2 d\phi^2 \right), \quad (4.6a)$$

$$f(r) = \frac{r^2}{\ell^2} + m^2(1 - \mathcal{A}^2 r^2), \quad (4.6b)$$

$$\Omega(r, \phi) = \mathcal{A}r \cos(m\phi) - 1. \quad (4.6c)$$

Though the metric (4.6) resembles the Class  $I_{\text{pushed}}$  metric (4.1), it describes the geometry of a black hole being pulled by a string, whose tension

$$\tau_\pi = \frac{1}{4\pi} m \mathcal{A} \sin(m\pi) \quad (4.7)$$

is positive [24].

In the rapid acceleration regime, there is a Killing horizon at

$$r_h = \frac{m\ell}{\sqrt{m^2 \mathcal{A}^2 \ell^2 - 1}}, \quad (4.8)$$

and the conformal boundary is found at

$$r_{\text{conf}} = \frac{1}{\mathcal{A} \cos(m\phi)}. \quad (4.9)$$

We consider values of the radial coordinate restricted between the conformal boundary (4.8) and the horizon (4.9),  $r_{\text{conf}} < r < r_h$ . We remark that  $r < r_h$  ensures the positivity of the metric function  $f(r)$ , whereas  $r > r_{\text{conf}}$  ensures the positivity of the conformal factor  $\Omega(r, \phi)$ . The geometry of this solution is depicted in Figure 9.

A quantity of interest is the circumference of a closed loop of constant radial coordinate, given by

$$\int_{-\pi}^{\pi} d\phi \sqrt{g_{\phi\phi}} = \int_{-\pi}^{\pi} d\phi \frac{r}{\mathcal{A}r \cos(m\phi) - 1} = \frac{4r}{m\sqrt{\mathcal{A}^2 r^2 - 1}} \operatorname{arctanh} \left( \sqrt{\frac{\mathcal{A}r + 1}{\mathcal{A}r - 1}} \tan \left( \frac{m\pi}{2} \right) \right). \quad (4.10)$$

It was shown in [24] that (4.10) is a decreasing function of  $r$ . As such, closed loops near to the horizon are smaller than those close to the conformal boundary. Now we can identify the horizon  $r = r_h$  as a black hole horizon and we consider only  $r$  that satisfy  $0 < r_{\text{conf}} < r < r_h$ . We therefore interpret larger values of the coordinate  $r$  as being closer to the black hole horizon. The radial coordinate  $r$  is therefore physically unintuitive but a convenient coordinate for the purpose of calculation and comparison with the other C-metric classes.

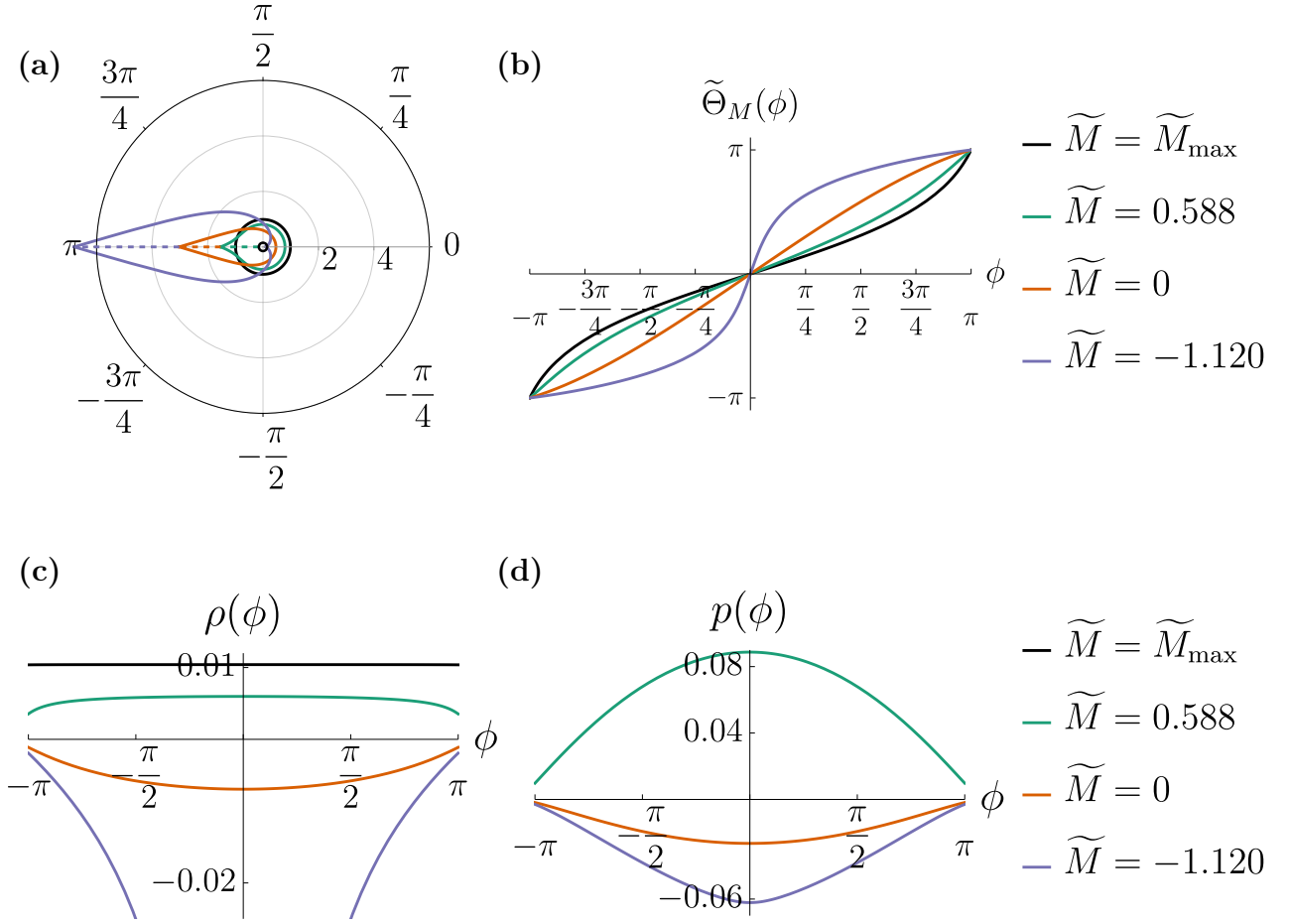


Figure 10: Class I<sub>C</sub> for  $r_0 = 0.3$ ,  $m = 0.25$ ,  $\mathcal{A} = 5.1$ ,  $\alpha = 0.25$ ,  $\ell = 1$  with  $\tilde{M}_{\min} = -\infty$ , and  $\tilde{M}_{\max} \approx 0.978$ . **(a)** Polar plot of shell radius  $\tilde{R}_M$  (2.36) over  $\phi \in (-\pi, \pi)$  for varying values of  $\tilde{M}$ ; dashed line indicates the string and the black ring represents the black hole. **(b)** Shell angular coordinate  $\tilde{\Theta}_M$  (2.36) for varying values of  $\tilde{M}$ . **(c)** Energy density of the shell as a function of the shell's intrinsic spatial coordinate  $\phi$  for varying values of  $\tilde{M}$ ; the curve for  $\tilde{M}_{\min}$  is diverges as  $1/\phi$  as  $\phi \rightarrow 0$ . **(d)** Pressure of the shell as a function of the shell's intrinsic coordinate  $\phi$  for varying values of  $\tilde{M}$ .

We summarise the constraints on the parameters  $\mathcal{A}$ ,  $m$ , and  $\ell$  as

$$m\mathcal{A}\ell > 1, \quad (4.11a)$$

$$0 < m < \frac{1}{2}, \quad (4.11b)$$

$$m\mathcal{A}\ell \sin(m\pi) < 1. \quad (4.11c)$$

Constraints (4.11a) and (4.11b) are necessary for the existence of the Class I<sub>C</sub> solution [24], whereas constraint (4.11c) ensures that  $r_h > r_{\text{conf}}$ . The physical properties of this black hole solution are described in [24].

The minimum value of the exterior mass parameter is given by

$$M_{\min} = \frac{f(r_0) (m^2 \mathcal{A}^2 \ell^2 \sin^2(m\phi_*) - 1)}{\alpha^2 (1 - \mathcal{A}r_0 \cos(m\phi_*))^2}, \quad (4.12a)$$



$$\phi_* = \begin{cases} 0 & \text{for } m \leq \frac{1}{\mathcal{A}\ell} \sqrt{\frac{\mathcal{A}r_0}{\mathcal{A}r_0-1}}, \\ \min \left\{ \frac{1}{m} \arccos \left( \frac{(m^2 \mathcal{A}^2 \ell^2 - 1) \mathcal{A} r_0}{m^2 \mathcal{A}^2 \ell^2} \right), \pi \right\} & \text{for } m > \frac{1}{\mathcal{A}\ell} \sqrt{\frac{\mathcal{A}r_0}{\mathcal{A}r_0-1}}. \end{cases} \quad (4.12b)$$

We note two special cases. First, for  $\phi_* = \frac{1}{m} \arccos \left( \frac{(m^2 \mathcal{A}^2 \ell^2 - 1) \mathcal{A} r_0}{m^2 \mathcal{A}^2 \ell^2} \right)$ , we have

$$M_{\min} = -\frac{m^2}{\alpha^2} (1 - m^2 \mathcal{A}^2 \ell^2) \quad (4.13)$$

whereas for  $\phi_* = 0$ , we have

$$M_{\min} = -\frac{f(r_0)}{\alpha^2 (1 - \mathcal{A} r_0)^2}. \quad (4.14)$$

In this case, with  $M = M_{\min}$ ,  $\rho(\phi) \propto -1/\phi$  near zero and hence  $\rho(\phi) \rightarrow -\infty$  as  $\phi \rightarrow 0$ . Furthermore, we have  $\widetilde{M} \rightarrow -\infty$  as  $M \rightarrow M_{\min}$ . This may be seen by noting that the integrand in the definition of  $\widetilde{M}$  (2.38) is even and so may be written over the interval  $\phi' \in (0, \pi)$ . For arbitrary values of  $M$ , the integrand is order unity near zero. However, for  $M = M_{\min}$  (4.14), the integrand is order  $1/\phi'$  near  $\phi' = 0$  and the integral diverges.

The shell constructed around the Class  $I_C$  solution is markedly different from that of the rapid acceleration phase of the Class  $I_{\text{pushed}}$  shell. We remark that  $\widetilde{M}_{\min} = -\infty$ ; hence, between the curves depicting the shell with  $\widetilde{M} = \widetilde{M}_{\min}$  and  $\widetilde{M} = 0$  lies the behaviour of the shell with global AdS exterior to the shell,  $\widetilde{M} = -1$ .

We plot the radial and angular coordinates of the shell in Figure 10 **(a)** and **(b)**. For small values of  $M$ , the shell resembles a teardrop with a pinch near the string at  $\phi = \pi$ . As  $M \rightarrow M_{\min}$ , the shell becomes cuspidal at  $\phi = 0$ , similar to the slow acceleration regime in the Class  $I_{\text{pulled}}$  solution depicted in Figure 2 **(a)**. However, as  $\beta_M$  diverges in this limit, the shell ADM radius  $\widetilde{R}_M$  also increases and the ADM angular coordinate becomes increasingly nonlinear. As  $\widetilde{M} \rightarrow \widetilde{M}_{\max}$ , the teardrop rounds off, but the angular coordinate remains nonlinear.

In Figure 10 **(c)** and **(d)**, we plot the shell energy density  $\rho$  and pressure  $p$ . The energy density and pressure may take any sign and increase with  $M$ . When the energy density and pressure are negative, they are maximised where the string meets the shell at  $\phi = \pi$ , whereas when the energy density and pressure are positive, they are maximised around  $\phi = 0$ . For  $M = M_{\min}$ , we have cut off the graph of the energy density so as to depict the other curves clearly; the energy density decreases, reaching a minimum at  $\phi = 0$  before increasing. As predicted in (2.51), the energy density and pressure are positive for large values of  $M$ , as  $\widetilde{M} \rightarrow \widetilde{M}_{\max}$ . We recall that  $p(\phi) \rightarrow \infty$  as  $\widetilde{M} \rightarrow \widetilde{M}_{\max}$ , hence this curve is not shown.

As the exterior spacetime mass  $M$  varies, we find both physical and unphysical solutions, depicted in Figure 10 **(c)**. Between the physical ( $\rho > 0$ ) and unphysical ( $\rho < 0$ ) shells, there exists a critical mass parameter  $M_{\text{crit}}$  for which the stress energy of the shell vanishes

$$M_{\text{crit}} := -\frac{m^2}{\alpha^2} (1 - m^2 \mathcal{A}^2 \ell^2). \quad (4.15)$$

In this case, physically there is no shell. However, the shell radial and angular functions are still regular for this critical exterior mass. We may therefore interpret this solution as a spacetime consisting of an accelerated black hole, pulled by a finite-length string at the end of which lies a point particle with mass  $\mu_\pi$  (2.28). The strong energy condition holds only for  $M > M_{\text{crit}}$ .

In Figure 11, we plot the mass of the point particle at the end of the string as a function of the exterior mass parameter  $M$ . We find that the mass is negative for all values of  $M$ , indicating

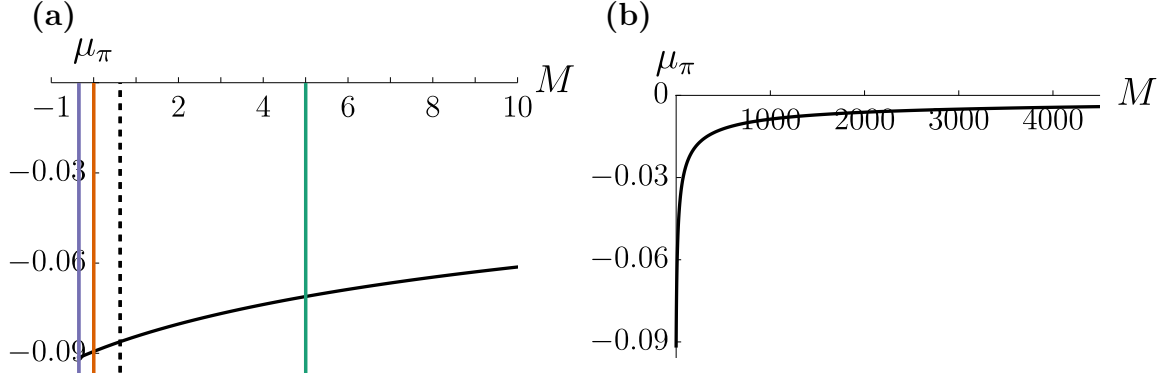


Figure 11: Class  $I_C$  for  $r_0 = 0.3$ ,  $m = 0.25$ ,  $\mathcal{A} = 5.1$ ,  $\alpha = 0.25$ ,  $\ell = 1$  with  $\widetilde{M}_{\min} = -\infty$ , and  $\widetilde{M}_{\max} \approx 0.978$ . **(a)** Plot of point particle mass  $\mu_\pi$  at  $\phi = \pm\pi$  (2.28) for varying values of  $M$ . Black vertical dashed line corresponds to  $M = M_{\text{crit}}$  (4.15). Coloured vertical lines correspond to the shells plotted in Figure 10. **(b)** Plot of point particle mass for larger range of  $M$  values, demonstrating the large- $M$  behaviour of  $\mu_\pi$  predicted in (2.54).

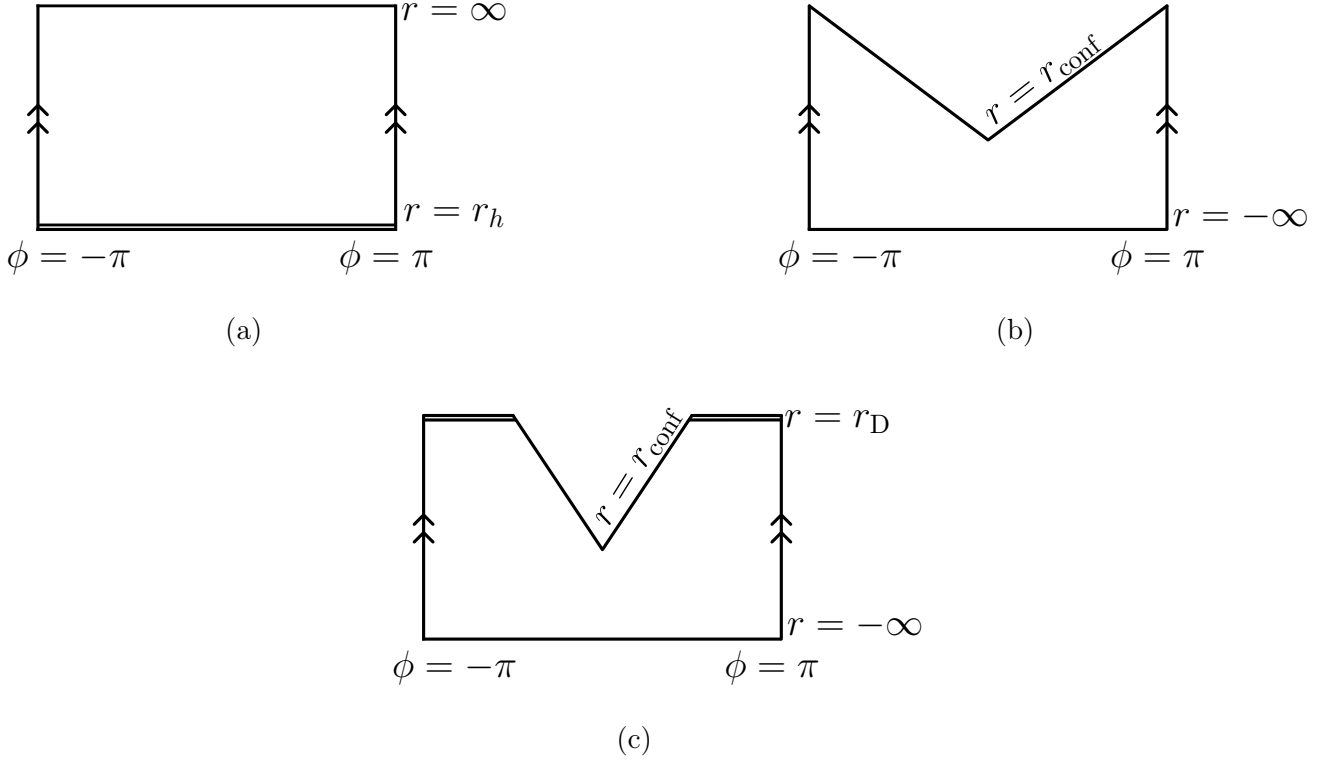


Figure 12: Constant time slice of the Class  $II_{\text{right}}$  solution. **(a)**  $r > 0$  patch. **(b)**  $r < 0$  patch, slow acceleration phase. **(c)**  $r < 0$  patch, rapid acceleration phase. Double lines in **(a)** and **(c)** represent a Killing horizon.

an angular excess at  $\phi = \pm\pi$ . As  $\widetilde{M} \rightarrow \widetilde{M}_{\max}$  ( $M \rightarrow \infty$ ), we see  $\mu_\pi \rightarrow 0$ . The negative mass of the point particle is in line with the negative tension of the string at  $\phi = \pm\pi$  in the Class  $I_{\text{pushed}}$  spacetimes, which include the Class  $I_C$  solution.

## 5. Class $\text{II}_{\text{right}}$

We consider now the Class  $\text{II}_{\text{right}}$  spacetime, describing a BTZ black hole pushed by a strut. In polar coordinates  $(\sigma, r, \phi)$ , the metric reads

$$ds_-^2 = \frac{1}{\Omega^2(r, \phi)} \left( -\frac{f(r)}{\alpha^2} d\sigma^2 + \frac{dr^2}{f(r)} + r^2 d\phi^2 \right), \quad (5.1a)$$

$$f(r) = \frac{r^2}{\ell^2} - m^2 (1 - \mathcal{A}^2 r^2), \quad (5.1b)$$

$$\Omega(r, \phi) = 1 + \mathcal{A}r \cosh(m\phi), \quad (5.1c)$$

where  $m > 0$ . We now obtain

$$\tau_\pi = -\frac{1}{4\pi} m \mathcal{A} \sinh(m\pi) \quad (5.2)$$

for the tension of the strut. Taking the limit  $\mathcal{A} \rightarrow 0$  and identifying  $m^2 = \alpha^2 M$  with  $M > 0$ , one recovers the geometry of a non-rotating BTZ black hole (2.5) in coordinates  $(\sigma, r, \phi) = (t, \alpha r_+, \theta/\alpha)$ .

The Class  $\text{II}_{\text{right}}$  spacetime is covered by two charts, one for  $r > 0$  and a second for  $r < 0$ , that are glued together across  $r = \pm\infty$ . We note that the proper distance to  $r = \pm\infty$  is finite,

$$\int_{\pm r_0}^{\pm\infty} dr \sqrt{g_{rr}} = \int_{\pm r_0}^{\pm\infty} dr \frac{1}{\sqrt{\Omega^2(r, \phi) f(r)}} < \infty, \quad (5.3)$$

for any fixed  $\phi$ . This follows from the asymptotic behaviour  $1/\sqrt{\Omega^2(r, \phi) f(r)} = \mathcal{O}(r^{-2})$  as  $r \rightarrow \infty$ . The stress energy of a shell formed in the  $r < 0$  chart is always unphysical and comprised of exotic matter. One may notice that for  $r < 0$ , the energy density in the large- $M$  limit is negative (2.51a).

The conformal boundary is located at

$$r_{\text{conf}} = -\frac{1}{\mathcal{A} \cosh(m\phi)}, \quad (5.4)$$

and the metric (5.1) has two Killing horizons

$$r_h = \frac{m\ell}{\sqrt{1 + m^2 \mathcal{A}^2 \ell^2}}, \quad (5.5a)$$

$$r_D = -\frac{m\ell}{\sqrt{1 + m^2 \mathcal{A}^2 \ell^2}}. \quad (5.5b)$$

The chart  $r > 0$  describes the exterior of a black hole with horizon at  $r = r_h$ . The Class  $\text{II}_{\text{right}}$  spacetime exhibits two phases of acceleration, slow and rapid, depending on the relative positions of  $r_D$  and  $r_{\text{conf}}$ . The rapid phase of acceleration is indicated by the presence of a Killing horizon in the  $r < 0$  chart.

The slow acceleration phase, defined by

$$m\mathcal{A}\ell \sinh(m\pi) < 1, \quad (5.6)$$

occurs when  $r_D$  is hidden behind the conformal boundary  $r_{\text{conf}}$ ,  $r < r_{\text{conf}} < r_D < 0$ . However, in the rapid acceleration phase, a ‘‘droplet’’ horizon – a noncompact horizon intersecting conformal infinity (also known as a black droplet) [36, 37, 24] – forms. The geometry of the Class  $\text{II}_{\text{right}}$  solution is depicted in Figure 12.

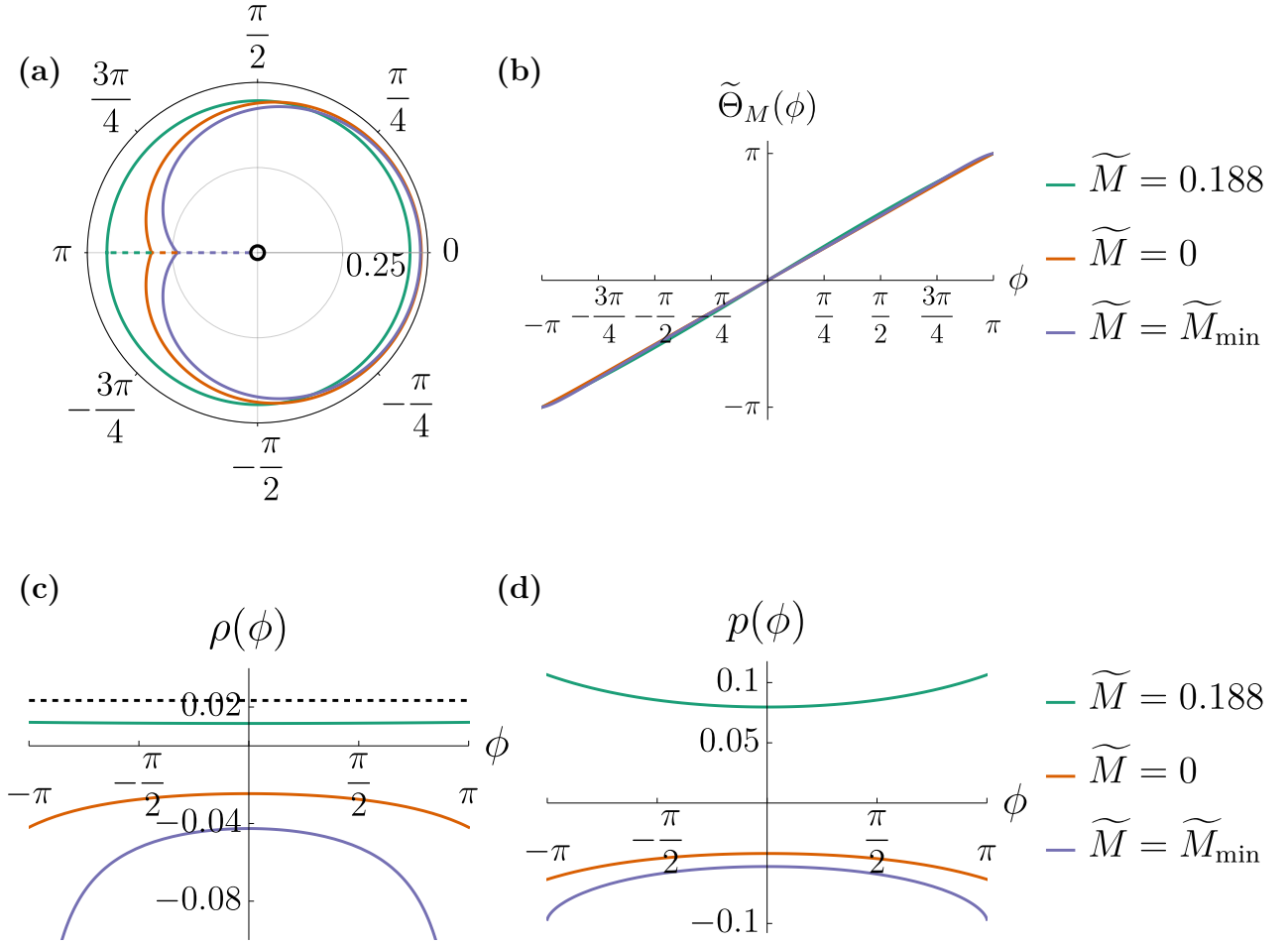


Figure 13: Class  $\text{II}_{\text{right}}$  ( $r > 0$ , slow phase) for  $r_0 = 0.6$ ,  $m = 0.5$ ,  $\mathcal{A} = 0.4$ ,  $\alpha = 0.25$ ,  $\ell = 1$ ,  $r_h \approx 0.490$  with  $\tilde{M}_{\min} \approx -0.203$ , and  $\tilde{M}_{\max} \approx 0.199$  (a) Polar plot of shell radius  $\tilde{R}_M$  (2.36) over  $\phi \in (-\pi, \pi)$  for varying values of  $\tilde{M}$ ; dashed line indicates the strut and black ring represents the black hole. (b) Shell angular coordinate  $\tilde{\Theta}_M$  (2.36) for varying values of  $\tilde{M}$ . (c) Energy density of the shell as a function of the shell's intrinsic spatial coordinate  $\phi$  for varying values of  $\tilde{M}$ . Black dashed line at asymptotic value as  $\tilde{M} \rightarrow \tilde{M}_{\max}$ . (d) Pressure of the shell as a function of the shell's intrinsic coordinate  $\phi$  for varying values of  $\tilde{M}$ .

The minimum value of the exterior mass parameter  $M$  depends on the chart. In the  $r > 0$  chart, the minimum value of the exterior mass parameter is given by

$$M_{\min} = \frac{f(r_0) (m^2 \mathcal{A}^2 \ell^2 \sinh^2(m\pi) - 1)}{\alpha^2 (1 + \mathcal{A} r_0 \cosh(m\pi))^2}, \quad (5.7)$$

which is negative in the slow acceleration regime and positive in the rapid acceleration regime.

### 5.1. Slow acceleration

We consider first the slow acceleration regime,  $m\mathcal{A}\ell \sinh(m\pi) < 1$ . We remark that in the  $r > 0$  chart, we have  $\tilde{M}_{\min} = 0$ ; hence the  $\tilde{M} = \tilde{M}_{\min}$  plot depicts a shell with an exterior geometry of Torricelli's trumpet. In this  $r < 0$  chart, however, we have  $\tilde{M}_{\min} < -1$ ; hence, between the

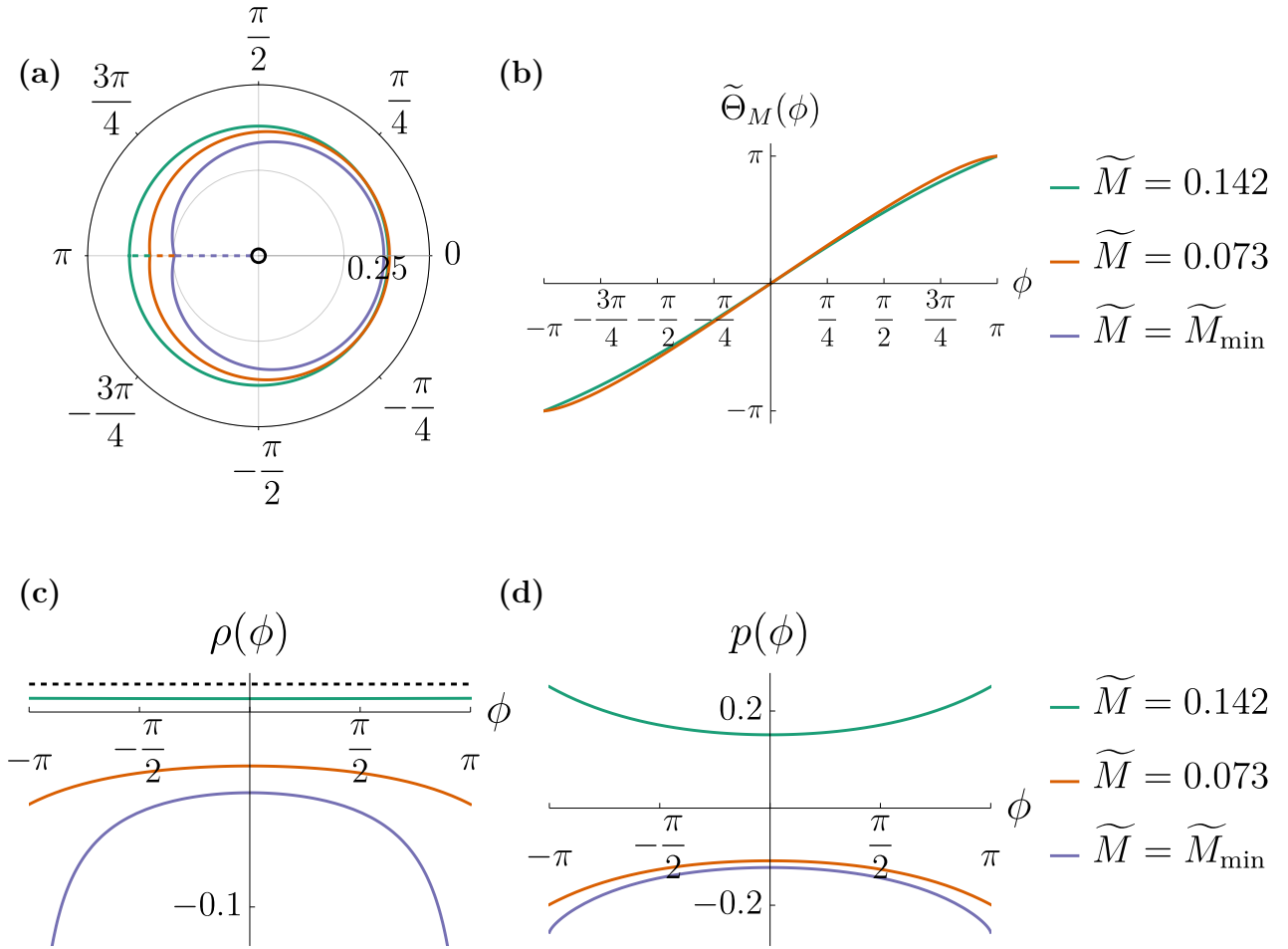


Figure 14: Class  $\text{II}_{\text{right}}$  ( $r > 0$ , rapid phase) for  $r_0 = 0.6$ ,  $m = 0.6$ ,  $\mathcal{A} = 0.6$ ,  $\alpha = 0.25$ ,  $\ell = 1$ ,  $r_h \approx 0.565$  with  $\widetilde{M}_{\text{min}} \approx 0.052$ , and  $\widetilde{M}_{\text{max}} \approx 0.144$ . **(a)** Polar plot of shell radius  $\widetilde{R}_M$  (2.36) over  $\phi \in (-\pi, \pi)$  for varying values of  $\widetilde{M}$ ; dashed line indicates the strut and black ring represents the black hole. **(b)** Shell angular coordinate  $\widetilde{\Theta}_M$  (2.36) for varying values of  $\widetilde{M}$ . **(c)** Energy density of the shell as a function of the shell's intrinsic spatial coordinate  $\phi$  for varying values of  $\widetilde{M}$ . Black dashed line at asymptotic value as  $\widetilde{M} \rightarrow \widetilde{M}_{\text{max}}$ . **(d)** Pressure of the shell as a function of the shell's intrinsic coordinate  $\phi$  for varying values of  $\widetilde{M}$ .

curves depicting the shell with  $\widetilde{M} = \widetilde{M}_{\text{min}}$  and  $\widetilde{M} = 0$ , there exists a shell whose exterior is global AdS,  $\widetilde{M} = -1$ .

We plot in Figure 13 **(a)** and **(b)** the shell radial and angular coordinates (2.36) as functions of the shell's intrinsic coordinate  $\phi$ . For small values of  $M$ , the shell resembles a cardioid with a true cusp where the strut (indicated by the dashed line) meets the shell at  $\phi = \pi$ . As  $\widetilde{M} \rightarrow \widetilde{M}_{\text{max}}$ , the shell becomes less deformed and tends to a circular shape, as expected from (2.47). The angular coordinate exhibits very little deviation from linearity.

As shown in Figure 13 **(c)** and **(d)**, the energy density  $\rho$  and pressure  $p$  of the shell may take either sign. For  $\rho, p > 0$ , the energy density and pressure are maximised where the strut meets the shell at  $\phi = \pi$ , whereas for  $\rho, p < 0$ , the energy density and pressure are maximised opposite the cusp, at  $\phi = 0$ . Both the energy density and pressure increase with  $M$ . Over the range of  $M$  we find both physical ( $\rho > 0$ ) and unphysical ( $\rho < 0$ ) shells. Between these, we find

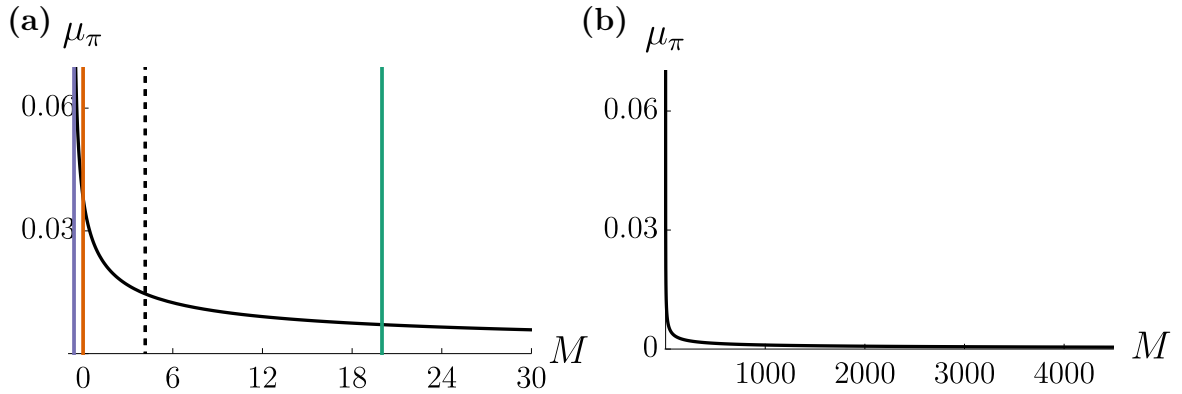


Figure 15: Class  $\text{II}_{\text{right}}$  ( $r > 0$ , slow phase) for  $r_0 = 0.6$ ,  $m = 0.5$ ,  $\mathcal{A} = 0.4$ ,  $\alpha = 0.25$ ,  $\ell = 1$ ,  $r_h \approx 0.490$  with  $\widetilde{M}_{\text{min}} \approx -0.203$ , and  $\widetilde{M}_{\text{max}} \approx 0.199$  (a) Plot of point particle mass  $\mu_\pi$  at  $\phi = \pm\pi$  (2.28) for varying values of  $M$ . Black vertical dashed line corresponds to  $M = M_{\text{crit}}$  (5.8). Coloured vertical lines correspond to the shells plotted in Figure 13. (b) Plot of point particle mass for larger range of  $M$  values, demonstrating the large- $M$  behaviour of  $\mu_\pi$  predicted in (2.54).

a critical exterior mass parameter  $M_{\text{crit}}$ , for which the stress energy of the shell vanishes,

$$M_{\text{crit}} := \frac{m^2}{\alpha^2}(1 + m^2 \mathcal{A}^2 \ell^2). \quad (5.8)$$

Only for  $M > M_{\text{crit}}$  does the stress energy satisfy the strong energy condition. As  $\widetilde{M}$  increases, the energy density is more evenly distributed across the shell.

The similarity between (5.8) and the Class  $\text{I}_C$  critical mass (4.15) is noteworthy. As in the Class  $\text{I}_C$  case, there is no shell. We interpret this solution as a spacetime consisting of an accelerated black hole, pushed by a finite-length strut with a point particle of mass  $\mu_\pi$  (2.28) at its end.

In Figure 15, we plot the mass of this point particle as a function of the exterior mass parameter  $M$ . We find that  $\mu_\pi > 0$  for all values of  $M$ , indicating an angular deficit at  $\phi = \pm\pi$ . As  $\widetilde{M} \rightarrow \widetilde{M}_{\text{max}}$  ( $M \rightarrow \infty$ ), we see  $\mu_\pi \rightarrow 0$ . In contrast to the Class  $\text{I}_C$  solution, the point particle has positive mass, however the strut at  $\phi = \pm\pi$  in Class  $\text{II}_{\text{right}}$  spacetimes has negative tension.

In the limit of zero acceleration, the string tension and deficit mass vanish and the critical mass (5.8) tends to  $M_{\text{crit}} \rightarrow m^2/\alpha^2$ . As analysed in Section 2.6, this corresponds to the interior geometry matching the outer geometry in coordinates  $(\sigma, r, \phi) = (t, r_+ \alpha, \theta/\alpha)$  and one would expect no shell. A similar correspondence is not available, however, for the Class  $\text{I}_C$  critical mass because the Class  $\text{I}_C$  solution is disconnected from the BTZ black hole ( $\mathcal{A} > 2/\ell$  and one may not take the  $\mathcal{A} \rightarrow 0$  limit).

## 5.2. Rapid acceleration

The rapid acceleration phase has features quite similar to the slow phase. Results for the  $r > 0$  chart are shown in Figure 14 (a) to (d).

The cusp at  $\phi = \pi$  is noticeably less pronounced for small values of  $M$  than in the slow acceleration phase and the angular coordinate is more non-linear. The energy density and

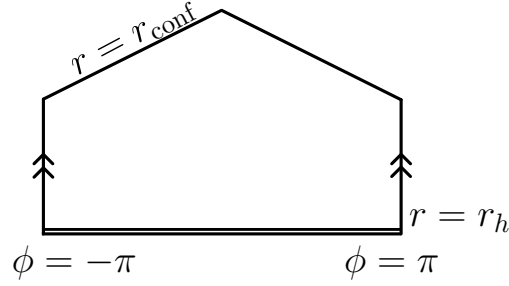


Figure 16: Constant time slice of the Class  $\text{II}_{\text{left}}$  solution. Double lines represent a Killing horizon.

pressure, however, are characteristically similar to the slow acceleration phase. In particular, for sufficiently large values of  $M$ , the strong energy condition is satisfied. Again, the shell vanishes for  $M = M_{\text{crit}}$  (5.8). The mass of the point particle is again positive and tends to zero as  $M \rightarrow \infty$ .

## 6. Class $\text{II}_{\text{left}}$

The Class  $\text{II}_{\text{left}}$  solution describes an accelerating BTZ black hole pulled by a string. The Class  $\text{II}_{\text{left}}$  metric is found by the mapping  $\mathcal{A} \rightarrow -\mathcal{A}$  in (5.1),

$$ds^2 = \frac{1}{\Omega^2(r, \phi)} \left( -\frac{f(r)}{\alpha^2} d\sigma^2 + \frac{dr^2}{f(r)} + r^2 d\phi^2 \right), \quad (6.1a)$$

$$f(r) = \frac{r^2}{\ell^2} - m^2 (1 - \mathcal{A}^2 r^2), \quad (6.1b)$$

$$\Omega(r, \phi) = 1 - \mathcal{A} r \cosh(m\phi) \quad (6.1c)$$

and

$$\tau_\pi = \frac{1}{4\pi} m \mathcal{A} \sinh(m\pi). \quad (6.2)$$

is the tension of the string.

The conformal boundary is found at

$$r_{\text{conf}} = \frac{1}{\mathcal{A} \cosh(m\phi)}. \quad (6.3)$$

The spacetime is covered by a single chart with  $r > 0$ . There is a single Killing horizon at

$$r_h = \frac{m\ell}{\sqrt{1 + m^2 \mathcal{A}^2 \ell^2}}. \quad (6.4)$$

To ensure  $r_h < r_{\text{conf}}$ , we require

$$m \mathcal{A} \ell \sinh(m\pi) < 1. \quad (6.5)$$

Therefore, there is no equivalent rapid phase of acceleration in the  $\text{II}_{\text{left}}$  solution. The geometry of this spacetime is depicted in Figure 16.

The minimum value of the exterior mass parameter is given by

$$M_{\min} = \frac{f(r_0)}{\alpha^2} \frac{(m^2 \mathcal{A}^2 \ell^2 \sinh^2(m\phi_*) - 1)}{(1 - \mathcal{A}r_0 \cosh(m\phi_*))^2}, \quad (6.6a)$$

$$\phi_* = \begin{cases} 0 & \text{for } m \leq \frac{1}{\mathcal{A}\ell} \sqrt{\frac{\mathcal{A}r_0}{1-\mathcal{A}r_0}}, \\ \min \left\{ \frac{1}{m} \operatorname{arccosh} \left( \frac{(m^2 \mathcal{A}^2 \ell^2 + 1) \mathcal{A}r_0}{m^2 \mathcal{A}^2 \ell^2} \right), \pi \right\} & \text{for } m > \frac{1}{\mathcal{A}\ell} \sqrt{\frac{\mathcal{A}r_0}{1-\mathcal{A}r_0}}. \end{cases} \quad (6.6b)$$

We note two special cases. First, for  $\phi_* = \frac{1}{m} \operatorname{arccosh} \left( \frac{(1+m^2 \mathcal{A}^2 \ell^2) \mathcal{A}r_0}{m^2 \mathcal{A}^2 \ell^2} \right)$ , we have

$$M_{\min} = \frac{m^2}{\alpha^2} (1 + m^2 \mathcal{A}^2 \ell^2). \quad (6.7)$$

Second, for  $\phi_* = 0$ , we have

$$M_{\min} = -\frac{f(r_0)}{\alpha^2 (1 - \mathcal{A}r_0)^2}. \quad (6.8)$$

In this case, with  $M = M_{\min}$ , we have  $\rho(\phi) \propto -1/\phi$  near zero and hence  $\rho(\phi) \rightarrow -\infty$  as  $\phi \rightarrow 0$ . Furthermore, we have  $\widetilde{M}_{\min} \rightarrow -\infty$  as  $M \rightarrow M_{\min}$  defined by (6.8). This may be seen by noting that the integrand in the definition of  $\widetilde{M}$  (2.38) is even and may be written over the interval  $\phi' \in (0, \pi)$ . For arbitrary values of  $M$ , the integrand is order unity near zero. However, for  $M = M_{\min}$  (6.8), the integrand is order  $1/\phi'$  near  $\phi' = 0$  and the integral diverges.

In Figure 17 (a) and (b), we plot the shell radial and angular coordinates as functions of the shell's intrinsic coordinate  $\phi$ . As  $M \rightarrow M_{\min}$ , the shell resembles a cardioid, pinched where the string meets the shell at  $\phi = \pi$  and with a cuspidal shape at  $\phi = 0$ . We note that in Figure 17 (a) though it appears graphically that the shell meets the horizon, this does not happen; in the interior spacetime, the shell is placed at  $r = r_0 > r_h$ , which is smoothly joined to the exterior spacetime coordinates.

As  $\widetilde{M} \rightarrow \widetilde{M}_{\max}$ , the shell becomes less deformed and tends to a teardrop shape, pinched at  $\phi = \pi$ . The angular coordinate  $\widetilde{\Theta}_M$  is strongly nonlinear for small values of  $M$  and becomes increasingly linear as  $\widetilde{M} \rightarrow 0$ ; however, the angular coordinate is nonlinear as  $\widetilde{M} \rightarrow \widetilde{M}_{\max}$ . We remark that  $\widetilde{M}_{\min} = -\infty$ ; hence, between the curves depicting the shell with  $\widetilde{M} = \widetilde{M}_{\min}$  and  $\widetilde{M} = 0$  there exists a shell whose exterior is global AdS, with  $\widetilde{M} = -1$ . As  $M \rightarrow M_{\min}$ , the ADM factor  $\beta_M$  diverges and the ADM shell radius  $\beta_M R_M(\phi)$  increases without bound.

We show plots of the shell energy density  $\rho$  and pressure  $p$  in Figure 17 (c) and (d). The energy density and pressure may both be positive or negative. For  $\rho, p < 0$ , the energy density and pressure are maximised where the string meets the shell at  $\phi = \pi$ . For  $\rho, p > 0$ , the energy density and pressure are maximised at  $\phi = 0$ . Both the energy density and pressure increase with  $M$  and are positive for sufficiently large  $M$ , as expected by (2.51). In Figure 17 (c), the graph of the energy density for  $\widetilde{M} = \widetilde{M}_{\min}$  is cut off to see the other curves clearly; as  $M_{\min}$  is given by (6.8) for the plotted parameters, the energy density diverges as  $\phi \rightarrow 0$ . The strong energy condition is satisfied for sufficiently large values of  $M$ .

As in Class II<sub>right</sub> and Class I<sub>C</sub>, we find a critical mass parameter between the physical ( $\rho > 0$ ) and unphysical ( $\rho < 0$ ) solutions for which the stress energy of the shell vanishes. The critical mass is (5.8) in both Class II<sub>right</sub> and Class II<sub>left</sub>, since each is obtained from the other by mapping  $\mathcal{A} \rightarrow -\mathcal{A}$  and the critical mass is quadratic in  $\mathcal{A}$ . For this choice of exterior mass parameter, the solution describes a spacetime consisting of an accelerated black hole, pulled by a finite-length string at whose end lies a point particle with mass  $\mu_\pi$  (2.28).



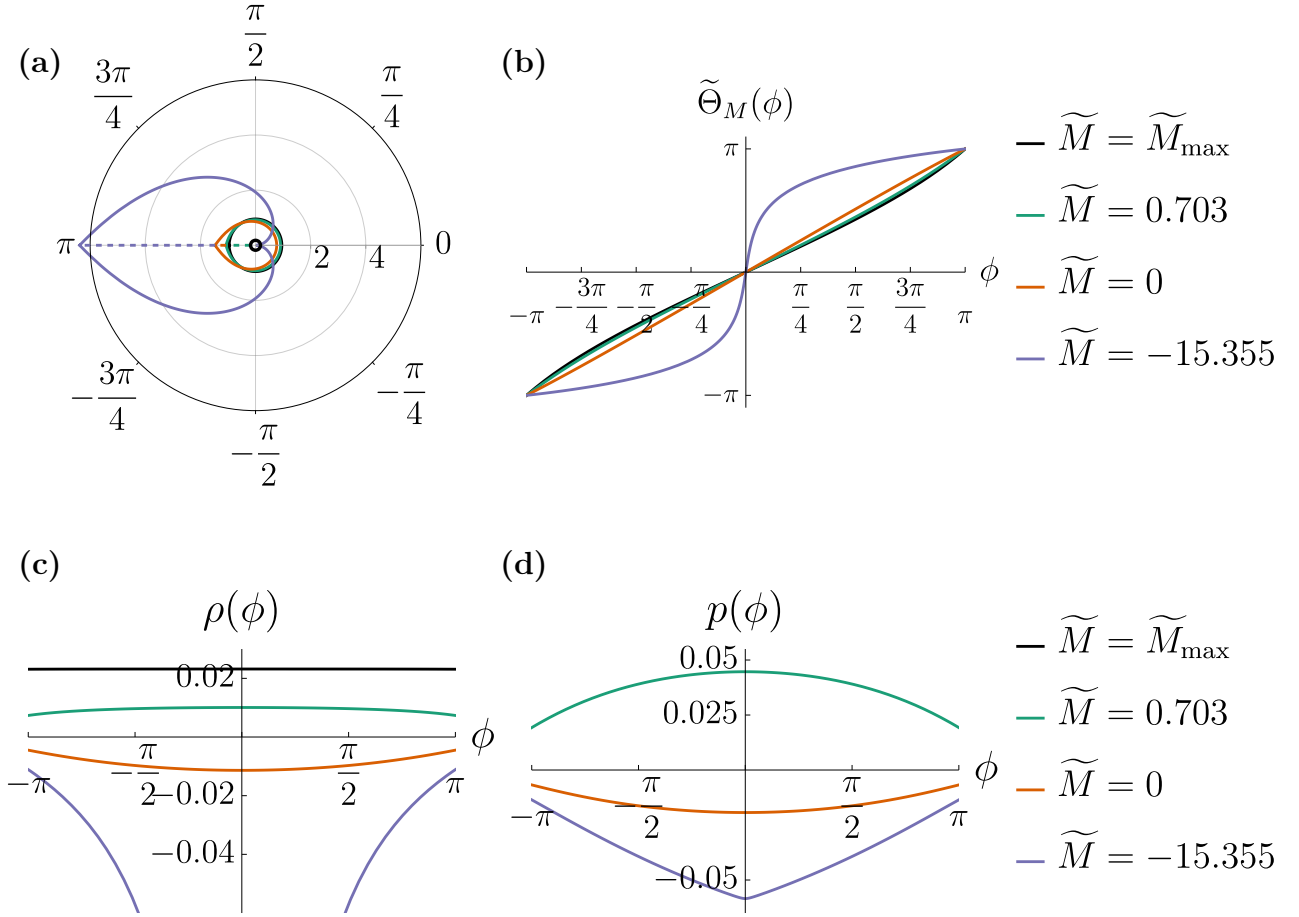


Figure 17: Class  $\text{II}_{\text{left}}$  for  $r_0 = 0.6$ ,  $m = 0.5$ ,  $\mathcal{A} = 0.4$ ,  $\alpha = 0.25$ ,  $\ell = 1$ ,  $r_h \approx 0.490$ , with  $\tilde{M}_{\min} = -\infty$ , and  $\tilde{M}_{\max} \approx 0.912$ . (a) Polar plot of shell radius  $\tilde{R}_M$  (2.36) over  $\phi \in (-\pi, \pi)$  for varying values of  $\tilde{M}$ ; dashed line indicates the string and black ring represents the black hole. (b) Shell angular coordinate  $\tilde{\Theta}_M$  (2.36) for varying values of  $\tilde{M}$ . (c) Energy density of the shell as a function of the shell's intrinsic spatial coordinate  $\phi$  for varying values of  $\tilde{M}$ . (d) Pressure of the shell as a function of the shell's intrinsic coordinate  $\phi$  for varying values of  $\tilde{M}$ .

In Figure 18, we plot the mass of this point particle as a function of the exterior mass parameter  $M$ . We find that the mass is negative for all values of  $M$ , indicating an angular excess at  $\phi = \pm\pi$ . As  $\tilde{M} \rightarrow \tilde{M}_{\max}$ , we see  $\mu_\pi \rightarrow 0$ . In contrast to the Class  $\text{I}_C$  solution, the point particle has negative mass, however the domain at  $\phi = \pm\pi$  in Class  $\text{II}_{\text{left}}$  spacetimes has positive tension.

## 7. Class III

We consider now the Class III spacetime, which has received the least attention in the literature. By making cuts in the spacetime and identifying two edges, one may form a double-strut solution [24]. This procedure, however, does not result in a periodic angular coordinate.

Instead, we consider two copies of the patch in the Class III spacetime from  $\phi = 0$  to  $\phi = \pi$ . In the second copy, we relabel the angular coordinate  $\phi \rightarrow -\phi$  and glue along the  $\phi = 0$  edges and identify the  $\phi = \pi$  and  $\phi = -\pi$  edges. This is now a periodic solution described by the

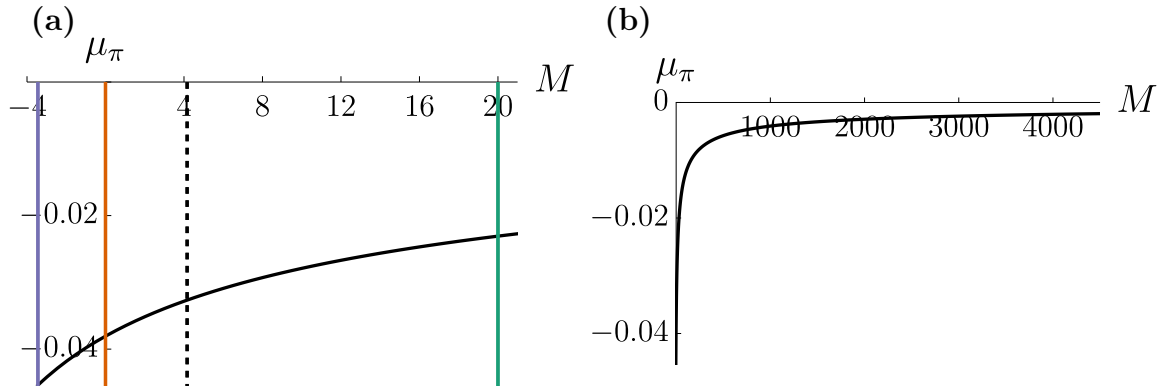


Figure 18: Class  $\text{II}_{\text{left}}$  for  $r_0 = 0.6$ ,  $m = 0.5$ ,  $\mathcal{A} = 0.4$ ,  $\alpha = 0.25$ ,  $\ell = 1$ ,  $r_h \approx 0.490$ , with  $\widetilde{M}_{\text{min}} = -\infty$ , and  $\widetilde{M}_{\text{max}} \approx 0.912$ . **(a)** Plot of point particle mass  $\mu_\pi$  at  $\phi = \pm\pi$  for varying values of  $M$ . Black vertical dashed line corresponds to  $M = M_{\text{crit}}$  (5.8). Coloured vertical lines correspond to the shells plotted in Figure 17. **(b)** Plot of point particle mass for larger range of  $M$  values, demonstrating the large- $M$  behaviour of  $\mu_\pi$ .

metric

$$ds^2 = \frac{1}{\Omega^2(r, \phi)} \left( -\frac{f(r)}{\alpha^2} d\sigma^2 + \frac{dr^2}{f(r)} + r^2 d\phi^2 \right), \quad (7.1a)$$

$$f(r) = \frac{r^2}{\ell^2} - m^2 (1 + \mathcal{A}^2 r^2), \quad (7.1b)$$

$$\Omega(r, \phi) = 1 + \mathcal{A}r |\sinh(m\phi)|. \quad (7.1c)$$

We call this solution the Class  $\text{III}_{\text{right}}$  spacetime.

### 7.1. Class $\text{III}_{\text{right}}$

This spacetime describes an accelerating black-hole being pushed by a strut at  $\phi = \pi$  and pulled by a string at  $\phi = 0$ . The corresponding strut/string tensions are

$$\tau_\pi = -\frac{m\mathcal{A}}{4\pi} \cosh(m\pi), \quad (7.2a)$$

$$\tau_0 = \frac{m\mathcal{A}}{4\pi}. \quad (7.2b)$$

Positivity of the metric function  $f(r)$  requires  $m\mathcal{A}\ell < 1$ . The conformal boundary is found at

$$r_{\text{conf}} = -\frac{1}{\mathcal{A} |\sinh(m\phi)|}. \quad (7.3)$$

The geometry of the periodic Class  $\text{III}_{\text{right}}$  is remarkably similar to that of the Class  $\text{II}_{\text{right}}$  spacetime. As in the Class  $\text{II}_{\text{right}}$  solution, this spacetime is covered two charts, one each for  $r > 0$  and  $r < 0$ , that are glued together across  $r = \pm\infty$ . This is motivated from the observation that the proper distance to  $r = \pm\infty$  is finite,

$$\int_{\pm r_0}^{\pm\infty} dr \sqrt{g_{rr}} = \int_{\pm r_0}^{\pm\infty} dr \frac{1}{\sqrt{\Omega^2(r, \phi) f(r)}} < \infty, \quad (7.4)$$

for any fixed  $\phi \neq 0$ . This follows from the asymptotic behaviour  $1/\sqrt{\Omega^2(r, \phi) f(r)} = \mathcal{O}(r^{-2})$  as  $r \rightarrow \infty$ . For  $\phi = 0$ , we have  $1/\sqrt{\Omega^2(r, \phi) f(r)} = \mathcal{O}(r^{-1})$  as  $r \rightarrow \infty$  and the proper length is

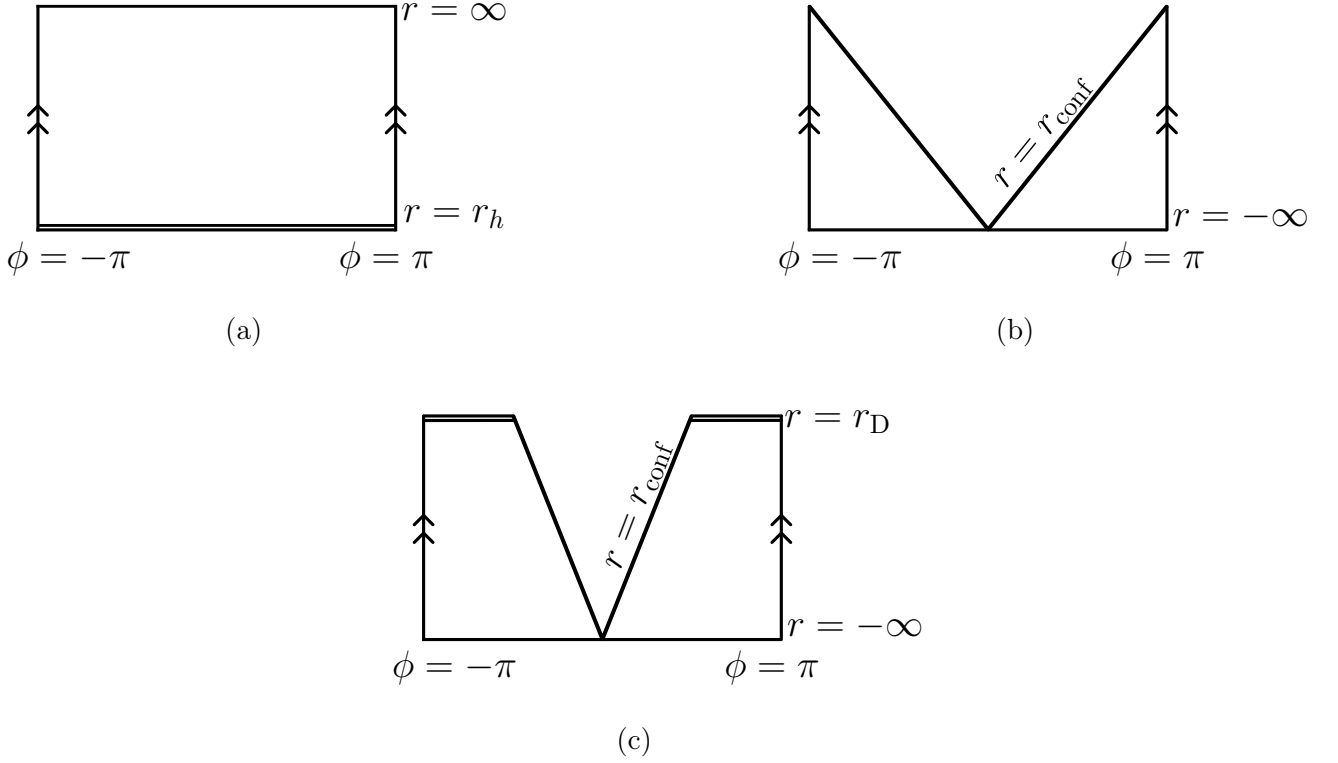


Figure 19: Constant time slice of the periodic Class III<sub>right</sub> solution. **(a)**  $r > 0$  patch. **(b)**  $r < 0$  patch, slow acceleration phase. **(c)**  $r < 0$  patch, rapid acceleration phase. Double lines in **(a)** and **(c)** represent a Killing horizon.

infinite. This may be seen in (19) as the point at which the conformal boundary meets  $r = -\infty$ . The stress energy of a shell formed in the  $r < 0$  chart is always unphysical and comprised of exotic matter. One may notice that for  $r < 0$ , the energy density in the large- $M$  limit is negative (2.51a).

There are two horizons,

$$r_h = \frac{m\ell}{\sqrt{1 - m^2 \mathcal{A}^2 \ell^2}}, \quad (7.5a)$$

$$r_D = -\frac{m\ell}{\sqrt{1 - m^2 \mathcal{A}^2 \ell^2}}, \quad (7.5b)$$

and the minimum value of the exterior mass parameter is given by

$$M_{\min} = \frac{f(r_0) (m^2 \mathcal{A}^2 \ell^2 \cosh^2(m\pi) - 1)}{\alpha^2 (1 + \mathcal{A}r_0 |\sinh(m\pi)|)^2}. \quad (7.6a)$$

The  $r > 0$  chart describes the exterior of a black hole whose horizon is at  $r = r_h$ . The  $r < 0$  chart exhibits two phases of acceleration, slow and rapid, depending on the relative positions of  $r_D$  and  $r_{\text{conf}}$ .

In the slow phase of acceleration, defined by

$$m\mathcal{A}\ell \cosh(m\pi) < 1, \quad (7.7)$$

the radial coordinate  $r$  is bounded between spatial infinity at  $r = -\infty$  and the conformal boundary,  $-\infty < r < r_{\text{conf}}$ . In the rapid acceleration phase, a droplet horizon forms — as in the Class II<sub>right</sub> rapid acceleration regime. The geometry of this solution is depicted in Figure 19.

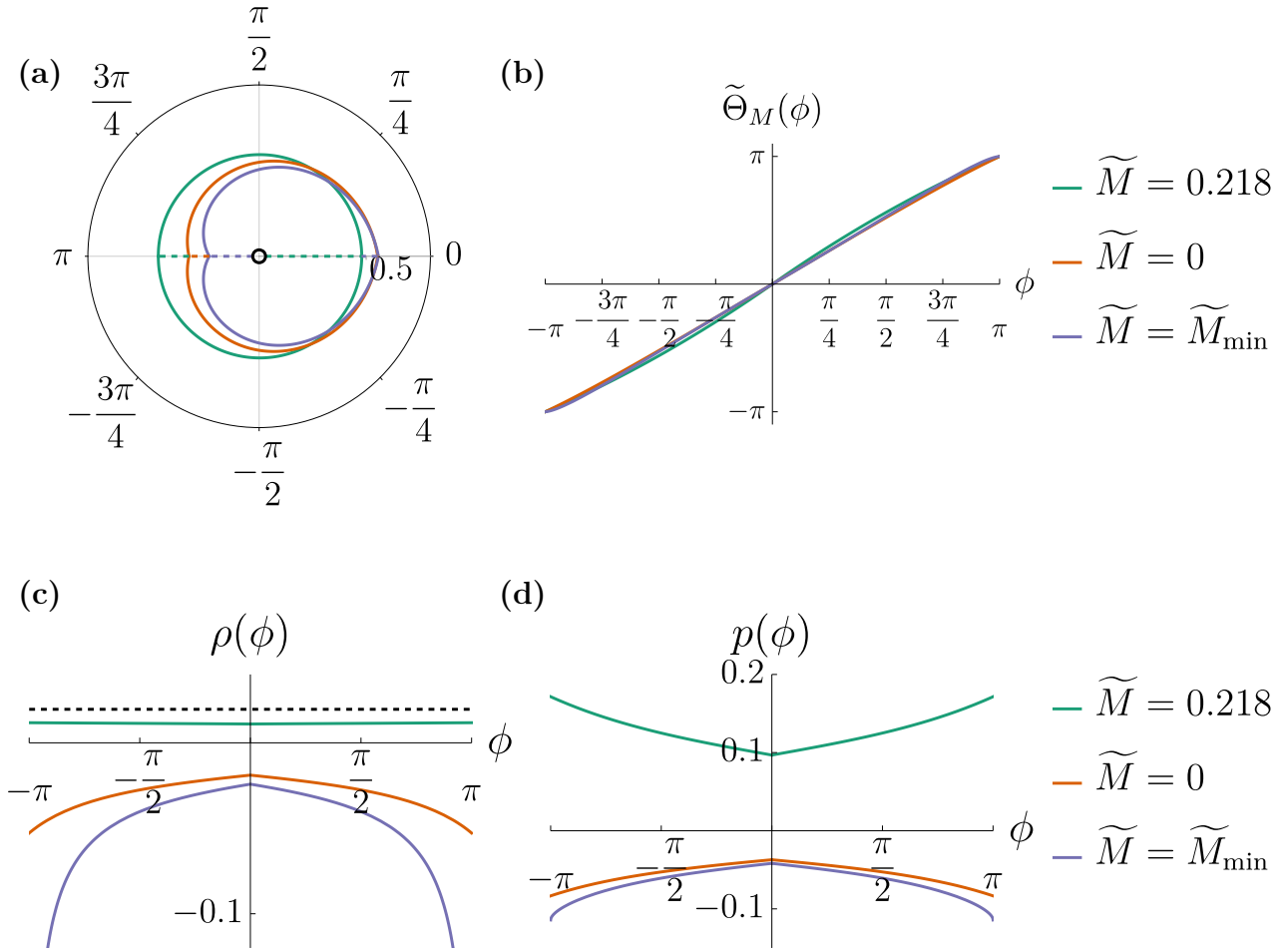


Figure 20: Periodic Class III<sub>right</sub> for  $r_0 = 0.6$ ,  $m = 0.5$ ,  $\mathcal{A} = 0.5$ ,  $\alpha = 0.25$ ,  $\ell = 1$ ,  $r_h \approx 0.516$  with  $\tilde{M}_{\min} \approx -0.084$ , and  $\tilde{M}_{\max} \approx 0.491$ . **(a)** Polar plot of shell radius  $\tilde{R}_M$  (2.36) over  $\phi \in (-\pi, \pi)$  for varying values of  $\tilde{M}$ ; dashed lines at  $\phi = 0, \pm\pi$  indicate the string and strut respectively and black ring represents the black hole. **(b)** Shell angular coordinate  $\tilde{\Theta}_M$  (2.36) for varying values of  $\tilde{M}$ . **(c)** Energy density of the shell as a function of the shell's intrinsic spatial coordinate  $\phi$  for varying values of  $\tilde{M}$ . Black dashed line at asymptotic value as  $\tilde{M} \rightarrow \tilde{M}_{\max}$ . **(d)** Pressure of the shell as a function of the shell's intrinsic coordinate  $\phi$  for varying values of  $\tilde{M}$ .

There is, however, a key distinction between the  $r < 0$  patches of the Class II<sub>right</sub> and the periodic Class III<sub>right</sub> solutions; in the periodic Class III<sub>right</sub> solution, the conformal boundary reaches spatial infinity at  $\phi = 0$ . As such, the  $r < 0$  patch has the spatial topology of (an open subset of)  $\mathbb{R}^2$ , rather than  $\mathbb{R} \times \mathbb{S}^1$ , and no closed loops of constant  $r$  may form. Because of this, we may not form a shell in the  $r < 0$  patch and we must restrict our attention to the  $r > 0$  black hole exterior.

In Figure 20 **(a)** and **(b)**, we plot the shell radial and angular coordinates as functions of the shell's intrinsic coordinate  $\phi$ . For small values of  $M$ , the shell resembles a cardioid and is pinched at  $\phi = 0$  with a cusp at  $\phi = \pi$ , at which points the string and strut (indicated by the dashed lines) meet the shell respectively. The shell becomes less deformed as  $\tilde{M} \rightarrow \tilde{M}_{\max}$ . The angular coordinate exhibits slight nonlinearities. We remark that  $\tilde{M}_{\min} = 0$ ; hence the  $\tilde{M} = \tilde{M}_{\min}$  plot depicts a shell with an exterior geometry of Torricelli's trumpet.

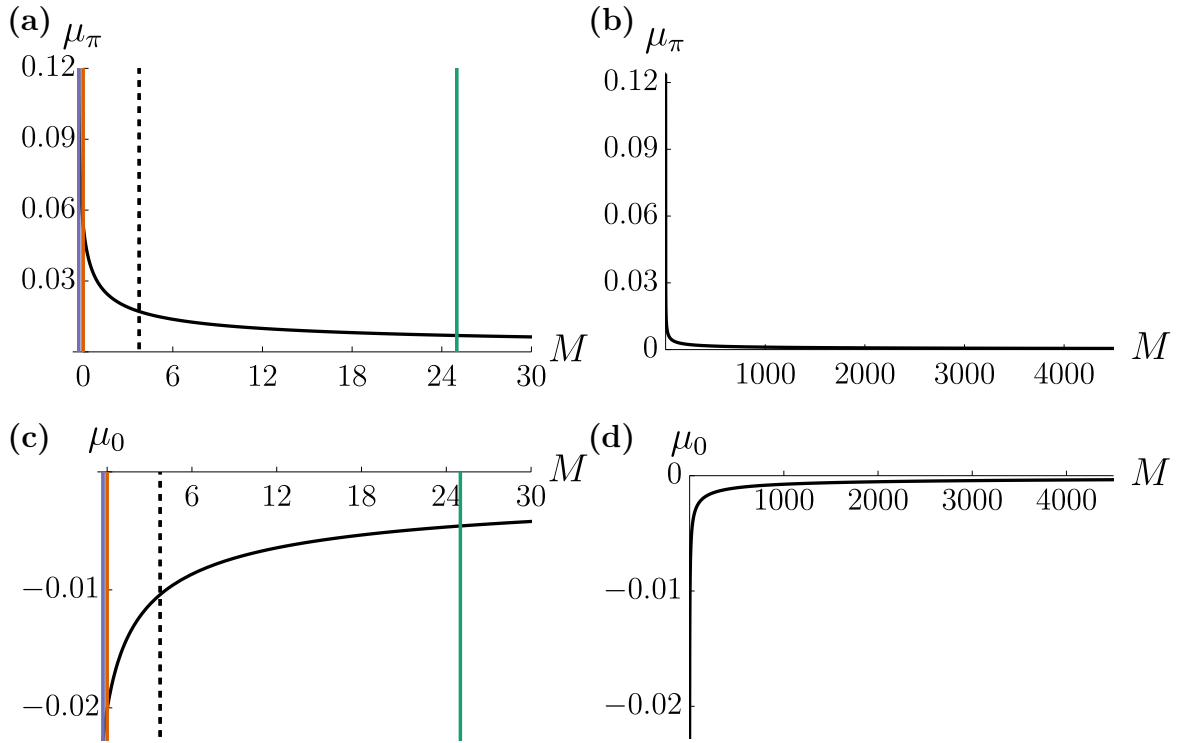


Figure 21: Periodic Class III<sub>right</sub> for  $r_0 = 0.6$ ,  $m = 0.5$ ,  $\mathcal{A} = 0.5$ ,  $\alpha = 0.25$ ,  $\ell = 1$ ,  $r_h \approx 0.516$  with  $\widetilde{M}_{\min} \approx -0.084$ , and  $\widetilde{M}_{\max} \approx 0.491$ . **(a)** Plot of point particle mass  $\mu_\pi$  at  $\phi = \pm\pi$  for varying values of  $M$ . Black vertical dashed line corresponds to  $M = M_{\text{crit}}$  (7.8). Coloured vertical lines correspond to the shells plotted in Figure 20. **(b)** Plot of point particle mass  $\mu_\pi$  for larger range of  $M$  values, demonstrating the large- $M$  behaviour of  $\mu_\pi$ . **(c)** Plot of point particle mass  $\mu_0$  at  $\phi = 0$  for varying values of  $M$ . Black vertical dashed line corresponds to  $M = M_{\text{crit}}$  (7.8). Coloured vertical lines correspond to the shells plotted in Figure 20. **(d)** Plot of point particle mass  $\mu_\pi$  for larger range of  $M$  values, demonstrating the large- $M$  behaviour of  $\mu_0$ .

In Figure 20 **(c)** and **(d)**, we plot the shell energy density  $\rho$  and pressure  $p$ , both of which may be positive or negative. For  $\rho, p < 0$ , the energy density and pressure are maximised at the pinch at  $\phi = 0$ . For  $\rho, p > 0$ , the energy density and pressure are maximised at  $\phi = \pi$ . As  $\widetilde{M} \rightarrow \widetilde{M}_{\max}$ , the energy density becomes evenly distributed across the shell, as anticipated by (2.51). The energy density and pressure increase with  $M$  and, as before, we find both physical ( $\rho > 0$ ) and unphysical ( $\rho < 0$ ) shells over the range of  $M$ . There is a critical exterior mass parameter  $M_{\text{crit}}$

$$M_{\text{crit}} := \frac{m^2}{\alpha^2}(1 - m^2 \mathcal{A}^2 \ell^2) \quad (7.8)$$

for which the stress energy of the shell vanishes, notably similar to the critical masses in Class I<sub>C</sub> (4.15), Class II (5.8), and Class III (7.8). Only for  $M > M_{\text{crit}}$  does the stress energy satisfy the strong energy condition. We interpret this solution as a spacetime consisting of an accelerated black hole, pushed by a finite-length strut at  $\phi = \pm\pi$  and pulled by a finite-length string at  $\phi = 0$ . At the ends of the respective strut and string lies a point particle with respective mass  $\mu_\pi$  (2.28) and  $\mu_0$  (2.33).

In Figure 21, we plot the mass of the point particle found at  $\phi = \pm\pi$  and at  $\phi = 0$  as functions of the exterior mass parameter  $M$ . We find that the point particle at  $\phi = \pm\pi$  has

positive mass, whereas the one at  $\phi = 0$  has negative mass, respectively indicating an angular deficit and excess. As in Class II, the sign of the point particles' mass is opposite to the corresponding string/strut's tension. As  $\widetilde{M} \rightarrow \widetilde{M}_{\max}$  ( $M \rightarrow \infty$ ), it is straightforward to show that  $\mu_\pi, \mu_0 \rightarrow 0$ .

### 7.2. Class III<sub>left</sub>

We find a second solution under the transformation  $\mathcal{A} \rightarrow -\mathcal{A}$ , the Class III<sub>left</sub> spacetime. This geometry is described by the metric

$$ds^2 = \frac{1}{\Omega^2(r, \phi)} \left( -\frac{f(r)}{\alpha^2} d\sigma^2 + \frac{dr^2}{f(r)} + r^2 d\phi^2 \right), \quad (7.9a)$$

$$f(r) = \frac{r^2}{\ell^2} - m^2 (1 + \mathcal{A}^2 r^2), \quad (7.9b)$$

$$\Omega(r, \phi) = 1 - \mathcal{A}r |\sinh(m\phi)| \quad (7.9c)$$

corresponding to an accelerating black-hole being pulled by a string at  $\phi = \pi$  and pushed by a strut at  $\phi = 0$ . The corresponding strut/string tensions are

$$\tau_\pi = \frac{m\mathcal{A}}{4\pi} \cosh(m\pi), \quad (7.10a)$$

$$\tau_0 = -\frac{m\mathcal{A}}{4\pi}. \quad (7.10b)$$

Positivity of the metric function  $f(r)$  requires  $m\mathcal{A}\ell < 1$ . The conformal boundary is found at

$$r_{\text{conf}} = \frac{1}{\mathcal{A} |\sinh(m\phi)|}. \quad (7.11)$$

There is a single Killing horizon at

$$r_h = \frac{m\ell}{\sqrt{1 - m^2 \mathcal{A}^2 \ell^2}}. \quad (7.12)$$

To ensure  $r_h < r_{\text{conf}}$ , we require

$$m\mathcal{A}\ell \cosh(m\pi) < 1. \quad (7.13)$$

Therefore, there is no equivalent rapid phase of acceleration in the III<sub>left</sub> solution. The geometry of this spacetime is depicted in Figure 22.

The minimum value of the exterior mass parameter is given by

$$M_{\min} = \frac{f(r_0)}{\alpha^2} \frac{(m^2 \mathcal{A}^2 \ell^2 \cosh^2(m\phi_*) - 1)}{(1 - \mathcal{A}r_0 \sinh(m\phi_*))^2}, \quad (7.14a)$$

$$\phi_* = \begin{cases} 0 & \text{for } m \leq \frac{1}{\mathcal{A}\ell} \sqrt{\frac{\mathcal{A}r_0(2 - \mathcal{A}r_0 \sinh(m\pi))}{2\mathcal{A}r_0 + (1 - \mathcal{A}^2 r_0^2) \sinh(m\pi)}}, \\ \pi & \text{for } m > \frac{1}{\mathcal{A}\ell} \sqrt{\frac{\mathcal{A}r_0(2 - \mathcal{A}r_0 \sinh(m\pi))}{2\mathcal{A}r_0 + (1 - \mathcal{A}^2 r_0^2) \sinh(m\pi)}}. \end{cases} \quad (7.14b)$$

We note that since  $m\mathcal{A}\ell \cosh(m\pi) < 1$  (7.13), we have  $M_{\min} < 0$ .

In the case  $\phi_* = 0$ , we have

$$M_{\min} = -\frac{(1 - m^2 \mathcal{A}^2 \ell^2) f(r_0)}{\alpha^2}, \quad (7.15)$$

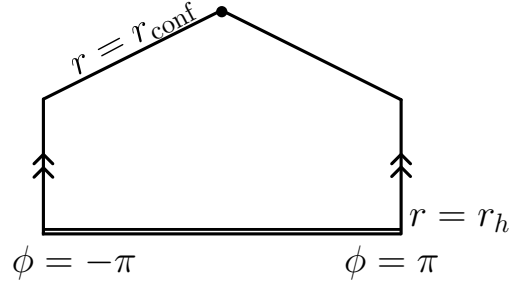


Figure 22: Constant time slice of the Class III<sub>left</sub> solution. Double lines represent a Killing horizon. Dot at  $\phi = 0$ , corresponds to  $r_{\text{conf}} = \infty$ .

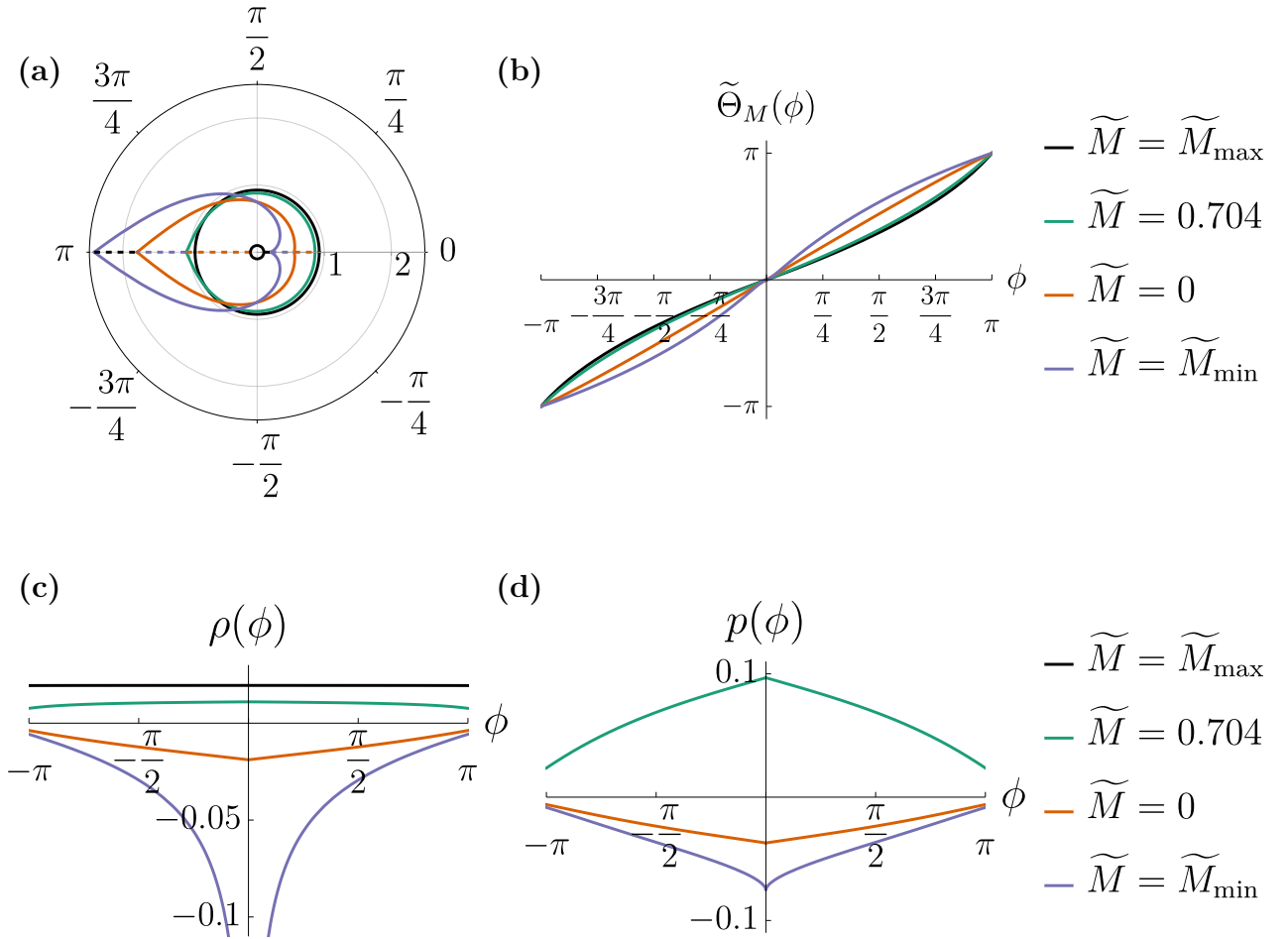


Figure 23: Periodic Class III<sub>left</sub> for  $r_0 = 0.6$ ,  $m = 0.5$ ,  $\mathcal{A} = 0.5$ ,  $\alpha = 0.25$ ,  $\ell = 1$ ,  $r_h \approx 0.516$  with  $\tilde{M}_{\text{min}} \approx -0.582$ , and  $\tilde{M}_{\text{max}} \approx 0.856$ . **(a)** Polar plot of shell radius  $\tilde{R}_M$  (2.36) over  $\phi \in (-\pi, \pi)$  for varying values of  $\tilde{M}$ ; dashed lines at  $\phi = 0, \pm\pi$  indicate the strut and string respectively and black ring represents the black hole. **(b)** Shell angular coordinate  $\tilde{\Theta}_M$  (2.36) for varying values of  $\tilde{M}$ . **(c)** Energy density of the shell as a function of the shell's intrinsic spatial coordinate  $\phi$  for varying values of  $\tilde{M}$ . Black dashed line at asymptotic value as  $\tilde{M} \rightarrow \tilde{M}_{\text{max}}$ . **(d)** Pressure of the shell as a function of the shell's intrinsic coordinate  $\phi$  for varying values of  $\tilde{M}$ .

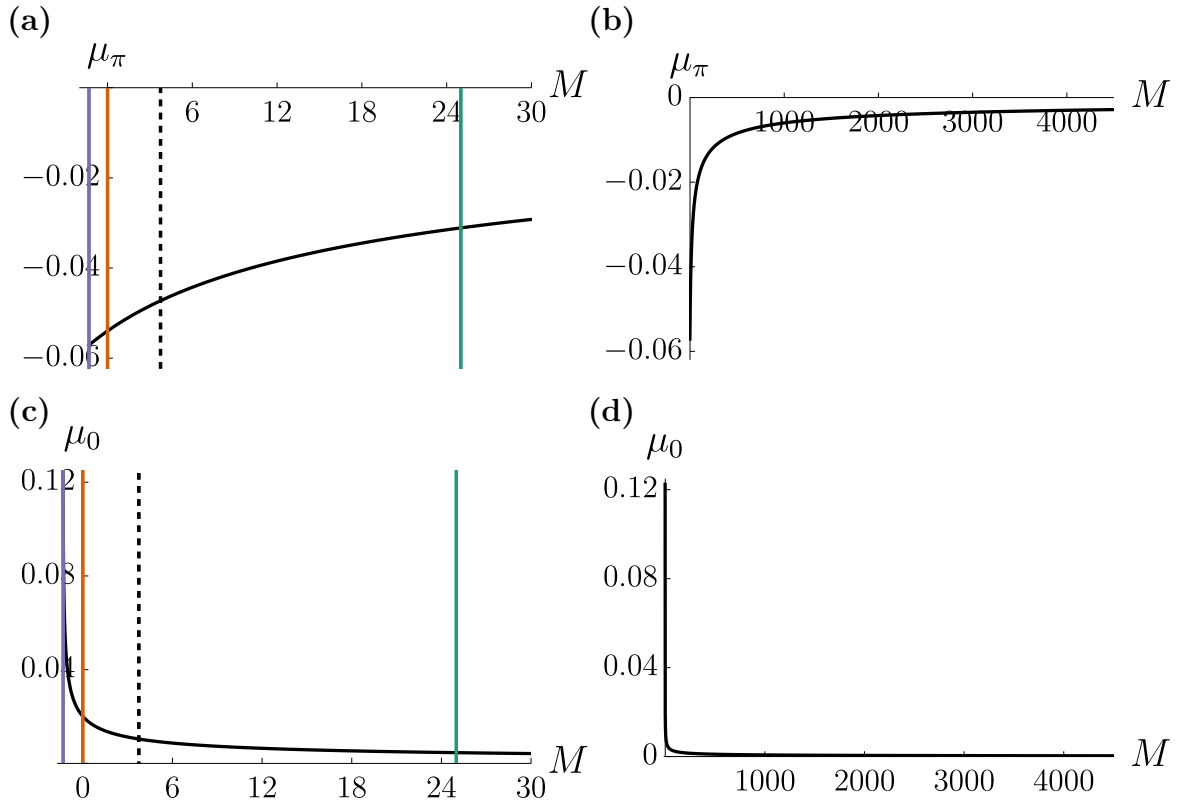


Figure 24: Periodic Class III<sub>left</sub> for  $r_0 = 0.6$ ,  $m = 0.5$ ,  $\mathcal{A} = 0.5$ ,  $\alpha = 0.25$ ,  $\ell = 1$ ,  $r_h \approx 0.516$  with  $\widetilde{M}_{\min} \approx -0.582$ , and  $\widetilde{M}_{\max} \approx 0.856$ . **(a)** Plot of point particle mass  $\mu_\pi$  at  $\phi = \pm\pi$  for varying values of  $M$ . Black vertical dashed line corresponds to  $M = M_{\text{crit}}$  (7.8). Coloured vertical lines correspond to the shells plotted in Figure 23. **(b)** Plot of point particle mass  $\mu_\pi$  for larger range of  $M$  values, demonstrating the large- $M$  behaviour of  $\mu_\pi$ . **(c)** Plot of point particle mass  $\mu_0$  at  $\phi = 0$  for varying values of  $M$ . The black vertical dashed line corresponds to  $M = M_{\text{crit}}$  (7.8). Coloured vertical lines correspond to the shells plotted in Figure 23. **(d)** Plot of point particle mass  $\mu_0$  for larger range of  $M$  values, demonstrating the large- $M$  behaviour of  $\mu_0$ .

at which value  $\rho(\phi) \rightarrow -\infty$  as  $\phi \rightarrow 0$ , a feature shared by the Class I<sub>C</sub> and Class II<sub>left</sub> solutions. However, unlike the Class I<sub>C</sub> and Class II<sub>left</sub> solutions,  $\widetilde{M}_{\min}$  remains finite.

In Figure 23 **(a)** and **(b)**, we plot the shell radial and angular coordinates as functions of the shell's intrinsic coordinate  $\phi$ . As  $M \rightarrow M_{\min}$ , the shell resembles a cardioid, pinched where the string meets the shell at  $\phi = \pi$  and with a cuspidal shape where the strut meets the shell at  $\phi = 0$ . Although in Figure 23 **(a)** it appears graphically that the shell meets the horizon, this does not actually happen: in the interior spacetime, the shell is placed at  $r = r_0 > r_h$ , which is smoothly joined to the exterior spacetime coordinates.

As  $\widetilde{M} \rightarrow \widetilde{M}_{\max}$ , the shell becomes less deformed and tends to a perfect circle. The angular coordinate  $\widetilde{\Theta}_M$  is strongly nonlinear for small values of  $M$  and becomes increasingly linear as  $\widetilde{M} \rightarrow 0$ , returning to nonlinearity as  $\widetilde{M} \rightarrow \widetilde{M}_{\max}$ . We remark that  $\widetilde{M}_{\min} = -\infty$ ; hence, between the curves depicting the shell with  $\widetilde{M} = \widetilde{M}_{\min}$  and  $\widetilde{M} = 0$  there exists a shell whose exterior is global AdS, with  $\widetilde{M} = -1$ .

We depict plots of the shell energy density  $\rho$  and pressure  $p$  in Figure 23 **(c)** and **(d)**. The energy density and pressure may both be positive or negative. For  $\rho, p < 0$ , the energy density and pressure are maximised where the string meets the shell at  $\phi = \pi$ . For  $\rho, p > 0$ , the energy



density and pressure are maximised at  $\phi = 0$ . Both the energy density and pressure increase with  $M$  and are positive for sufficiently large  $M$ , as expected by (2.51). In Figure 23 (c), the graph of the energy density for  $\widetilde{M} = \widetilde{M}_{\min}$  is cut off to see the other curves clearly; as  $M_{\min}$  is given by (7.15) for the plotted parameters, the energy density diverges as  $\phi \rightarrow 0$ . As in the Class III<sub>right</sub> solution, we find both physical  $\rho > 0$  and unphysical  $\rho < 0$  shells. Between these lies a solution with vanishing stress energy, there is no shell. As the Class III<sub>right</sub> and Class III<sub>left</sub> solutions are identified through the map  $\mathcal{A} \rightarrow -\mathcal{A}$ , the critical exterior mass parameter is again given by (7.8). Only for  $M > M_{\text{crit}}$  (7.8) does the stress energy satisfy the strong energy condition.

We interpret this solution as a spacetime consisting of an accelerated black hole, pushed by a finite-length strut at  $\phi = \pm\pi$  and pulled by a finite-length string at  $\phi = 0$  and at the respective ends of which lies a point particle with masses  $\mu_\pi$  (2.28) and  $\mu_0$  (2.33).

In Figure 24, we plot the masses of the point particles found at  $\phi = \pm\pi$  and at  $\phi = 0$  as functions of the exterior mass parameter  $M$ . We find that the point particle at  $\phi = \pm\pi$  has negative mass, whereas the one at  $\phi = 0$  has positive mass, indicating an angular deficit and excess respectively. As in Class II, the sign of the point particles' mass is opposite to the corresponding string/strut's tension. As  $\widetilde{M} \rightarrow \widetilde{M}_{\max}$  ( $M \rightarrow \infty$ ), we see  $\mu_\pi, \mu_0 \rightarrow 0$ .

## 8. Conclusions

We have carried out a comprehensive study of the C-metric in (2+1) dimensions, placing it inside a shell of stress energy and matching it to an exterior vacuum AdS metric. In contrast to nearly all studies of shell construction, the shells we obtain do not have circular symmetry. We have outlined the general construction in Section 2, where we find that the angular coordinate outside the shell is a nonlinear monotonically increasing function of the interior angular coordinate matched at the shell. This has the effect of giving the shell the shape of either a teardrop or a cardioid, depending on the parameters of the interior metric.

The Class I solutions respect the strong energy condition, regardless of whether they are pushed or pulled. Both the density and the pressure tend to be concentrated on the part of the shell farthest from the direction of acceleration: either away from the domain wall if pulled and near the domain wall if pushed.

An exception to this is the Class I<sub>C</sub> solutions, which corresponds to a rapid acceleration phase that is disconnected from the  $\mathcal{A} = 0$  BTZ black hole. These shells will violate the energy conditions for a sufficiently small mass parameter  $M < M_{\text{crit}}$ . For  $M = M_{\text{crit}}$  there is no shell: the black hole is pushed or pulled by a domain wall of finite length with a point particle at its end.

Class II shells likewise violate the energy conditions for sufficiently small mass. As with Class I<sub>C</sub>, the energy conditions are violated if the mass parameter  $M < M_{\text{crit}}$ ; if the interior is that of an accelerating point mass  $M < 0$  then the energy conditions are always violated. If the exterior mass has the critical value then the solution describes an accelerated black hole pulled by a finite-length string at whose end lies a point particle.

We also constructed two explicit classes of Class III shells, right and left, with the right exhibiting a slow and rapid phase of acceleration. These spacetimes consist of two patches that are glued together across  $r = \pm\infty$  in standard coordinates. For this class, the shells are restricted as to their size: only shells with  $0 < r < +\infty$  can be constructed.

Summarising, we have employed the thin-shell formalism to find not only cardioid and

teardrop shaped shells matching interior C-metric solutions to vacuum AdS solutions but to also find new solutions to Einstein's field equations that have no shells. These fall into three categories: an accelerated black hole pulled by a finite-length string with a point particle at the other end (Class I<sub>C</sub>, Class II<sub>left</sub>), an accelerated black hole pushed by a finite-length strut with a point particle at the other end (Class II<sub>right</sub>), and an accelerated black hole pushed from one side by a finite-length strut and pulled from the other by a finite-length string, each with a point particle at the other end (Class III<sub>right</sub>, Class III<sub>left</sub>).

Our results should prove useful for several different further investigations. First, as noted in the introduction, our work can be extended to the rotating case. By choosing a sufficiently small shell, we can construct (2+1)-dimensional rotating C-metric solutions in the interior that do not have superluminal domain walls. Second, our results can be extended to (3 + 1) dimensions, surrounding the black hole and a portion of the string/strut with a cardioid/teardrop shell having two spatial dimensions. A third problem would be that of gravitational collapse of the shells we have constructed, to see the resultant fate of the spacetime.

## Acknowledgments

We thank Jorma Louko for helpful discussions on aspects of this project. The work of CRDB during the writing of this manuscript was supported by ESPRC (EP/W524402/1). This work was supported in part by the Natural Sciences and Engineering Research Council of Canada.

## References

- [1] Levi-Civita T 1917 *Atti Accad. Naz. Lincei, Cl. Sci. Fis., Mat. Nat., Rend.* **26** 307
- [2] Weyl H 1918 *Ann. Phys. (Leipzig)* **59** 185
- [3] Kinnersley W and Walker M 1970 **2** 1359–1370
- [4] Bonnor W B 1983 **15** 535–551
- [5] Mann R B and Ross S F 1995 **52** 2254 (*Preprint gr-qc/9504015*)
- [6] Podolský J 2002 *Czech. J. Phys.* **52** 1–10 (*Preprint gr-qc/0202033*)
- [7] Dias O J C and Lemos J P S 2003 *Phys. Rev. D* **67** 084018 (*Preprint hep-th/0301046*)
- [8] Plebański J F and Demiański M 1976 **98** 98–127
- [9] Dowker F, Gauntlett J P, Kastor D A and Traschen J H 1994 *Phys. Rev. D* **49** 2909–2917 (*Preprint hep-th/9309075*)
- [10] Anabalón A, Appels M, Gregory R, Kubizňák D, Mann R B and Ovgün A 2018 *Phys. Rev. D* **98** 104038 (*Preprint 1805.02687*)
- [11] Anabalón A, Gray F, Gregory R, Kubizňák D and Mann R B 2019 *JHEP* **04** 096 (*Preprint 1811.04936*)
- [12] Gregory R and Scoins A 2019 *Phys. Lett. B* **796** 191–195 (*Preprint 1904.09660*)
- [13] Abbasvandi N, Cong W, Kubiznak D and Mann R B 2019 *Class. Quant. Grav.* **36** 104001 (*Preprint 1812.00384*)
- [14] Abbasvandi N, Ahmed W, Cong W, Kubizňák D and Mann R B 2019 *Phys. Rev. D* **100** 064027 (*Preprint 1906.03379*)
- [15] Ahmed W, Chen H Z, Gesteau E, Gregory R and Scoins A 2019 *Class. Quant. Grav.* **36** 214001 (*Preprint 1906.10289*)
- [16] Gregory R, Lim Z L and Scoins A 2021 *Front. in Phys.* **9** 187 (*Preprint 2012.15561*)
- [17] Ball A and Miller N 2021 *Class. Quant. Grav.* **38** 145031 (*Preprint 2008.03682*)
- [18] Emparan R, Horowitz G T and Myers R C 2000 *JHEP* **01** 007 (*Preprint hep-th/9911043*)
- [19] Emparan R, Horowitz G T and Myers R C 2000 *JHEP* **01** 021 (*Preprint hep-th/9912135*)
- [20] Emparan R, Frassino A M and Way B 2020 *JHEP* **11** 137 (*Preprint 2007.15999*)
- [21] Feng Y, Ma H, Mann R B, Xue Y and Zhang M 2024 *JHEP* **08** 184 (*Preprint 2404.07192*)
- [22] Climent A, Emparan R and Hennigar R A 2024 (*Preprint 2404.15148*)
- [23] Astorino M 2011 *JHEP* **01** 114 (*Preprint 1101.2616*)

- [24] Arenas-Henriquez G, Gregory R and Scoins A 2022 *JHEP* **05** 063 (*Preprint* 2202.08823)
- [25] Arenas-Henriquez G, Cisterna A, Diaz F and Gregory R 2023 *JHEP* **09** 122 (*Preprint* 2308.00613)
- [26] Oppenheimer J R and Snyder H 1939 *Phys. Rev.* **56**(5) 455–459 URL <https://link.aps.org/doi/10.1103/PhysRev.56.455>
- [27] Ross S F and Mann R B 1993 *Phys. Rev. D* **47** 3319–3322 (*Preprint* hep-th/9208036)
- [28] Mann R B and Oh J J 2006 *Phys. Rev. D* **74** 124016 [Erratum: *Phys.Rev.D* 77, 129902 (2008)] (*Preprint* gr-qc/0609094)
- [29] Cisterna A, Diaz F, Mann R B and Oliva J 2023 *JHEP* **11** 073 (*Preprint* 2309.05559)
- [30] Banados M, Teitelboim C and Zanelli J 1992 *Phys. Rev. Lett.* **69** 1849–1851 (*Preprint* hep-th/9204099)
- [31] Banados M, Henneaux M, Teitelboim C and Zanelli J 1993 *Phys. Rev. D* **48** 1506–1525 [Erratum: *Phys.Rev.D* 88, 069902 (2013)] (*Preprint* gr-qc/9302012)
- [32] Carlip S 1995 *Class. Quant. Grav.* **12** 2853–2880 (*Preprint* gr-qc/9506079)
- [33] Casals M, Fabbri A, Martínez C and Zanelli J 2019 *Phys. Rev. D* **99** 104023 (*Preprint* 1902.01583)
- [34] Israel W 1966 *Nuovo Cim. B* **44S10** 1 [Erratum: *Nuovo Cim.B* 48, 463 (1967)]
- [35] Ashtekar A and Varadarajan M 1994 *Phys. Rev. D* **50**(8) 4944–4956 URL <https://link.aps.org/doi/10.1103/PhysRevD.50.4944>
- [36] Hubeny V E, Marolf D and Rangamani M 2010 *Class. Quant. Grav.* **27** 025001 (*Preprint* 0909.0005)
- [37] Hubeny V E, Marolf D and Rangamani M 2010 *Class. Quant. Grav.* **27** 095015 (*Preprint* 0908.2270)